*Review*

# Recent Advances in Photoelectrochemical Sensors for Analysis of Toxins and Abused Drugs in the Environment

Yan Mao, Xiaoxin Liu, Yu Bao * and Li Niu

Center for Advanced Analytical Science, Guangzhou Key Laboratory of Sensing Materials and Devices, Guangdong Engineering Technology Research Center for Photoelectric Sensing Materials and Devices, c/o School of Chemistry and Chemical Engineering, Guangzhou University, Guangzhou 510006, China; ymao@gzhu.edu.cn (Y.M.); lniu@gzhu.edu.cn (L.N.)
* Correspondence: baoyu@gzhu.edu.cn

**Abstract:** Toxic pollutants in the environment, such as toxins and abused drugs, have posed a major threat to human health and ecosystem security. It is extremely desirable to develop simple, low-cost, sensitive, and reliable techniques for the detection of these pollutants in the environment. As a booming analytical method, photoelectrochemical (PEC) sensors possess low background noise and high sensitivity. The performances of PEC sensors are fundamentally related to the photoelectric conversion efficiency, which mainly depends on the properties of photoactive materials. This review aims to summarize the engineered photoactive materials, i.e., semiconductors and semiconductor-based heterojunctions, as well as their actual applications, with emphasis on sensing mechanisms in PEC sensors for the analysis of toxins and abused drugs in the environment. Finally, the future research perspectives in this field are also discussed.

**Keywords:** photoelectrochemical sensors; toxins; abused drugs; semiconductor heterojunction

## 1. Introduction

Increasingly serious environmental pollution is a worldwide problem which is caused by the rapid industrialization and urbanization of the past few decades. There are many toxic pollutants in the environment, such as toxins and abused drugs, which pose a major threat to human health and ecosystem security [1,2]. Microcystins are a class of toxins mainly produced by cyanobacteria, and microcystin-leucine arginine (MC–LR) is the kind of freshwater toxin with the strongest toxicity and greatest potential to do harm; it brings many accidents and threats to human health because it is a powerful inhibitor of two key enzymes, protein phosphatases type 2A and type 1, in cellular processes [3–5]. The World Health Organization (WHO) proposed that the maximum allowable amount in drinking water be stipulated as $1 \mu g \ L^{-1}$ for MC–LR [6].

Abused drugs are a new kind of environmental pollutant. With their continuous release into the environment, the global environmental burden and ecological risk are increasing [2,7,8]. Non-steroidal anti-inflammatory drugs (NSAIDs) are a category of drugs. Although they possess analgesic, antipyretic, and anti-inflammatory effects, they are also considered harmful to human health and ecosystem security [9–11]. Therefore, NSAIDs are regarded as a new pollutant by the WHO. As reported, NSAIDs and other abused drugs such as antibiotics and antioxidants are frequently detected in the aquatic systems [12,13]. Consequently, it is extremely desirable and urgent to develop sensitive and reliable techniques for the detection of toxins and abused drug pollutants in the environment.

Various analytical techniques, including a variety of chromatographic techniques [14–16], enzyme-linked immunosorbent assays [17–19], and spectrophotometric techniques [20,21], are frequently used for sensitive determination of toxins and abused drugs. However, the requirements of tedious sample pretreatment, skilled operators, and expensive and precise instruments greatly limit their application scope and in situ applications. Therefore, it is of

great significance to develop a low-cost and convenient routine analysis method for toxins and abused drugs in the environment.

New emerging photoelectrochemical sensors (PEC sensors) are sensors based on the principle of photoelectric chemistry for the analysis and detection of biological and chemical molecules; they refer to the process of generating current by causing valence electron transfer inside the photoexcited material and triggering the chemical reaction under the irradiation of a light source [22–27]. Since light and photocurrents are used as excitation sources and recognition signals, respectively, PEC sensors can reduce background noise and achieve higher sensitivity than other conventional technologies. In addition, the use of an electronic reader makes PEC instruments simple, cost-effective, and miniaturized [28]. These obvious characteristics make the PEC sensors possible candidate sensors for the rapid and accurate monitoring of toxins and abused drugs in the environment.

Photoelectric conversion efficiency generally has a great influence on the sensitivity of the PEC sensors, which mainly depends on the properties of photoactive materials [29,30]. The photoactive materials under light irradiation can cause charge separation and transfer, and subsequently generate photocurrent as the detection signal, which usually acts as the conversion layer in the conversion of photons to electric energy [31]. Up to now, reviews have focused on the processes of PEC-sensor technology and its application in various environmental pollutants [28,30,32–36]. However, as far as we know, there is no integral overview of PEC sensors for monitoring toxins and abused drugs in the environment. Herein, this paper summarizes the applications of photoactive materials in PEC sensors in the analysis of toxins and abused drugs in the environment in recent years. In addition, the challenges and future prospects in this field are also discussed. We hope to provide some insights into the development of more mature PEC sensor strategies in order to meet the actual needs of toxins and abused drugs monitoring in the environment.

## 2. Principle of PEC Sensors

Typical PEC sensors mainly consist of three parts: an excitation light source, a detection system containing an electrolyte and electrode, and a signal acquisition system. Photoactive materials are applied as a photoelectric converter at the interface of a working electrode to produce photocurrent signals under light irradiation. The properties of photoactive materials or the electrolyte environment can be directly or indirectly changed by the target analytes, resulting in photocurrent variation and quantitative analysis [32].

As shown in Figure 1, a semiconductor photoactive materials-modified conductive substrate induces electron–hole ($e^-$-$h^+$) pairs under light irradiation in a typical PEC sensing process. The holes on the valence band (VB) transfers to the conduction band (CB). Correspondingly, an electrochemical workstation could measure the photocurrent signal that originated from the separation and migration of photogenerated charge carriers. In accordance with the electron migration direction, the photocurrent signal can be divided into anode sensing, corresponding to the photoinduced electrons transfer from the electrode to an external circuit, triggering a redox reaction with electron donors (D) by photoinduced holes; meanwhile, the inverse leads to a cathodic sensing via electron acceptors (A), trapping the excited electrons from the CB. Based on the different formation process of photocurrents at the interface, PEC sensing involves three main principles: one is that the analyte is directly used as an electron donor or acceptor, and feasible PEC detection is achieved through a simple redox strategy [37,38]; the other concerns observing the quantitative response change of the photocurrent via the indirect physical and chemical interaction between the targets and the photoactive materials modified by the recognition elements (such as aptamers [6,39–41], antibodies [42,43], and molecularly imprinted polymers [44,45]) to effectively indicate the concentration of the targets; the last one is the space effect-based sensing, i.e., that the analyte molecules interact with the photoactive materials to form a complex, contributing to a steric hindrance effect on the charge transform between interfaces and an enhanced recombination of $e^-$-$h^+$ pairs [46,47].
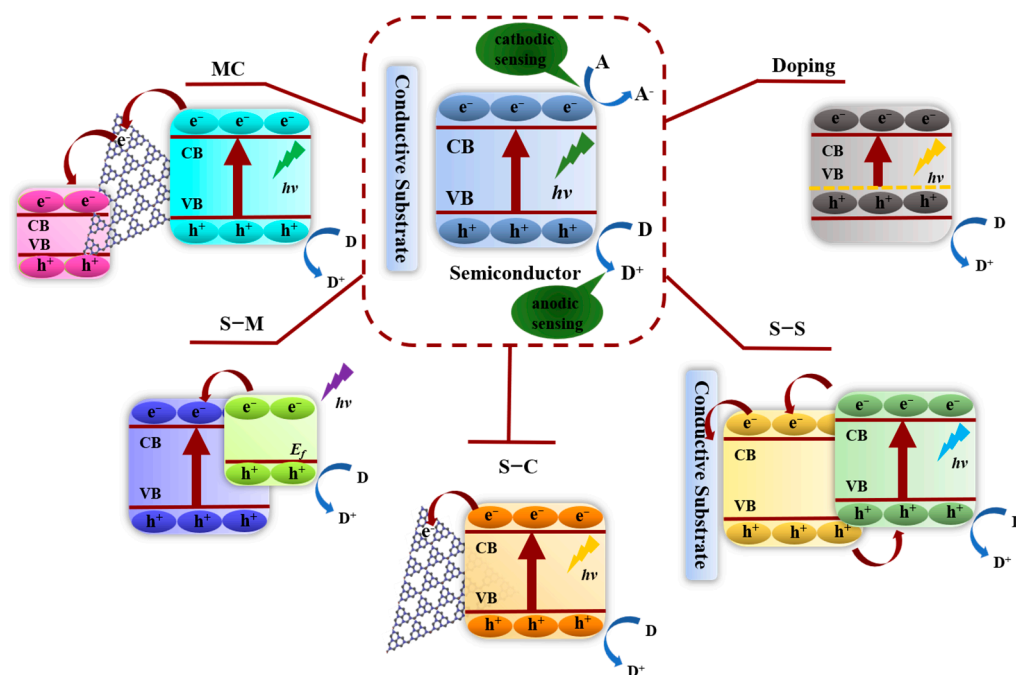
**Figure 1.** Schematic diagram of a typical PEC sensor based on semiconductor photoactive materials.

### 3. Photoactive Materials in PEC Sensors for Analysis of Toxins and Abused Drugs in the Environment

Photoactive materials act as a transducer converting the interactions between the analytes and PEC active materials, which play a crucial role in the PEC sensing system and demonstrate superior light capture capabilities, satisfactory charge separation efficiency, and appropriate energy level [37]. Excellent photoactive nanomaterials with high photoelectric conversion efficiency can greatly contribute to the excellent analytical performance of PEC sensors [48]. According to previous reports, photoactive materials can be divided into semiconductor and semiconductor-based heterojunctions. The semiconductor-based heterojunctions can effectively increase the photoelectric conversion efficiency of photoactive materials by means of heterojunctions, which usually have the following four categories, semiconductor–semiconductor heterojunctions (S–S heterojunctions), semiconductor–carbon heterojunctions (S–C heterojunctions), semiconductor–metal heterojunctions (S–M heterojunctions) and multi-component heterojunctions (MC heterojunctions), as shown in Figure 1. In addition, PEC sensing is based on anodic sensing as an example.

#### 3.1. Semiconductors

Based on their good band gap alignment, controllable size, and excellent biological compatibility, a wide range of semiconductor materials, such as metal oxides [49–52], metal chalcogenides [53,54], Bi-based semiconductor materials [55–57], graphite-like carbon nitride (g-C$_3$N$_4$) [58,59], and organic polymers [60,61], have attracted enormous interest in the construction of PEC sensors for the analysis of toxins and abused drugs in the environment. However, owing to the short absorption threshold, high e$^-$-h$^+$ recombination rate, and mismatch of band structure, the photoelectron production efficiency is low, which seriously hinders the feasibility of a single semiconductor. For example, Li et al. developed a photoelectrochemical detector for the determination of organic compounds based on the excellent oxidation power of nanostructured TiO$_2$ photoanodes, which stemmed from the photo-hole generated under UV illumination [62]. Chen et al. fabricated a novel, simple, high-sensitivity, and high-selectivity MC–LR photoelectrochemical sensor on highly ordered and vertically aligned TiO$_2$ nanotubes with molecularly imprinted polypyrrole (PPy) as the recognition element under a UV lamp [49]. Highly ordered and vertically

aligned TiO$_2$ nanotubes exhibit a sensitive photo-oxidation current due to their outstanding photocatalytic ability. PPy can recognize the MC–LR targets via the multiple hydrogen bond interactions. Then, the $\pi$ bond delocalized electron system of PPy facilitates the separation of photogenerated electron–hole pairs and improves the photoelectric conversion efficiency that would enhance the PEC current response. Özcan et al. used commercial TiO$_2$-modified FTO electrodes for the photoelectrochemical determination of paracetamol under three UV fluorescent lamps [63]. As UV light only accounts for about 3–4% of solar energy on earth [64], it is necessary to reduce the band gap of single semiconductor, such as TiO$_2$ (3.2 eV) and ZnO (3.4 eV) [65], to make the photoactive materials exhibit high visible light responsive activity for the useful utilization of solar energy.

Element doping can be regarded as a simple and effective approach to adjusting the PEC performances of semiconductors [66,67], which narrows the bandgap energy of semiconductors and shifts the threshold wavelength to the visible light region because of changes in the nanocrystal electronic structure [68]. Wang et al. successfully grew novel Ti$^{3+}$ self-doped branched rutile TiO$_2$ nanorod arrays (NRAs) on FTO transparent conductive glass [69]. The Ti$^{3+}$ defects in the TiO$_2$ nanoparticles, the related oxygen vacancies, as well as the nanobranch structure, expended the optical absorption of the TiO$_2$ NRAs from 400 nm to 510 nm. The doped and branched TiO$_2$ NRAs with larger specific surface areas and stronger light absorption could significantly improve their photoelectrochemical properties. Li et al. constructed co-doped ZnO diluted magnetic semiconductor (DMS) for fabricating PEC aptasensors of acetamiprid (Figure 2a) [70]. On account of the *sp-d* exchange interactions between the band electron and the localized *d* electrons of Co$^{2+}$, Co$^{2+}$ doping is beneficial in expanding the optical absorption bandwidth of ZnO to the visible region and promoting the separation of photogenerated carriers. The linear range of the fabricated aptasensor for acetamiprid was 0.5–800 nmol L$^{-1}$, and the detection limit was 0.18 nmol L$^{-1}$. Zheng et al. fabricated a boron and graphene quantum dots-co-doped g-C$_3$N$_4$ (named GBCN) as a dopamine PEC sensor, which showed a low detection limit of 0.96 nM, a wide detection range of 0.001–800 μM, and good stability (no obvious photocurrent change was found both after 20 light source on/off cycles and 90-day storage), as shown in Figure 2b [71]. The excellent properties of the fabricated PEC-active material might be due to the following reasons: (1) GBCN has more dopamine active adsorption sites with the obviously increased specific surface area of g-C$_3$N$_4$ after co-doping; (2) co-doping makes the adsorption red shift from 470 to 540 nm and increases the absorption intensity; (3) the synergistic effect of boron and graphene quantum dots effectively promotes the migration of photogenerated electrons from the conduction band of g-C$_3$N$_4$ to graphene quantum dots, as well as facilitating charge separation.

Oxygen vacancies [48,72–75] and nitrogen vacancies [76] have also been reported to increase the charge separation efficiency and broaden the light adsorption range. Naldoni et al. synthesized novel crystalline core/disordered shell black TiO$_2$ nanoparticles (NPs) with a reduced bandgap of only 1.85 eV, which could fit for visible light absorption, as shown in Figure 3 [72]. The experimental data analysis shows that oxygen vacancies are present in the bulk anatase crystalline phase, while the disordered NP surface appears to be nearly stoichiometric. Whereas, the experimental data analysis also proves that the narrowing of the bandgap is caused by the synergistic existence of oxygen vacancies and surface disorder. Cui et al. utilized the synergistic effect between the oxygen vacancies concentration and lattice strain of BiOBr nanosheets in order to improve the photoelectric response [74]. Yan et al. developed a ciprofloxacin (CIP) PEC sensor by using nitrogen-deficient graphitic carbon nitride (ND-g-CN) as a PEC-active material [76]. Nitrogen vacancies can be served as charge traps to effectively suppress the charge recombination, which works in conjunction with the 2D thin-sheet structures of the available charge separation and transfer to increase light capture and enhance PEC performance. The detection range of the designed PEC sensor for CIP is 60 to 19,090 ng L$^{-1}$, and the detection limit is 20 ng L$^{-1}$.
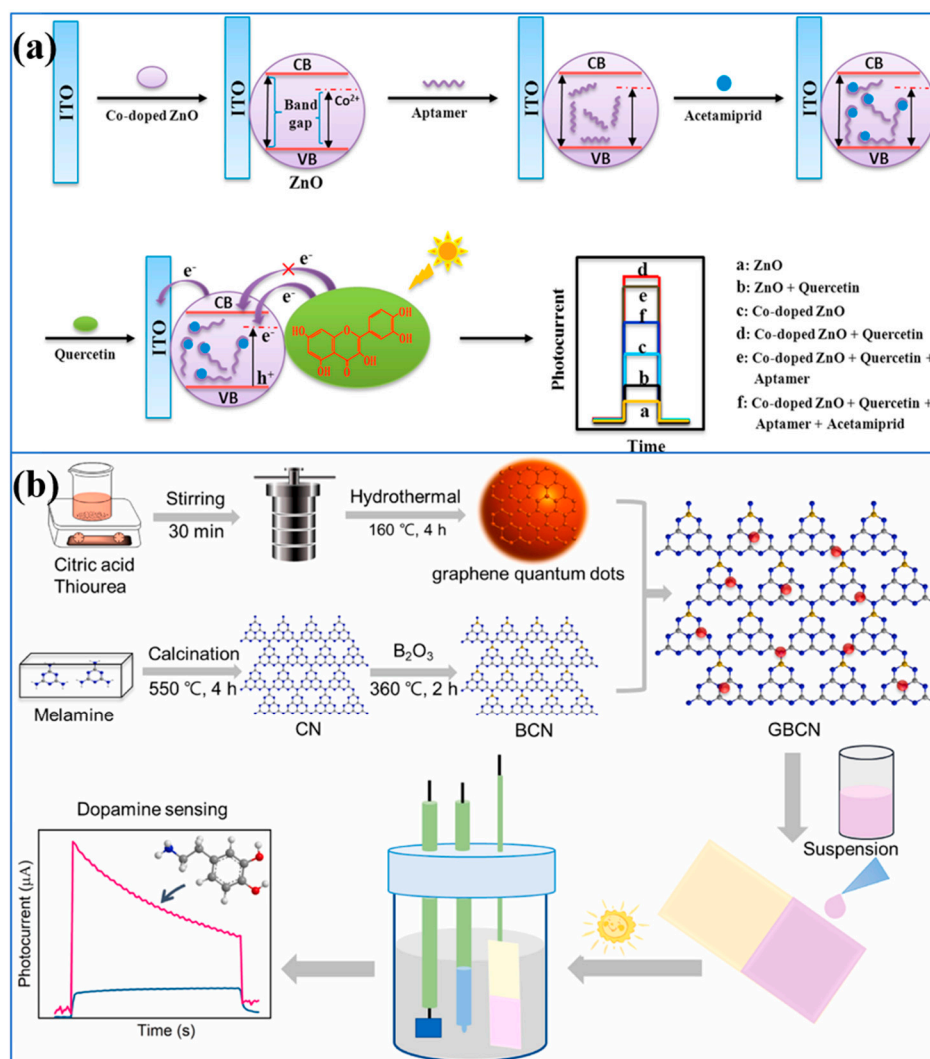
**Figure 2.** (**a**) The schematic diagram of the fabricated PEC aptasensor based on co-doped ZnO DMS coupled with acetamiprid aptamer [70]. (**b**) The boron and graphene quantum dots co-doped g-C3N4 as dopamine PEC sensor [71].
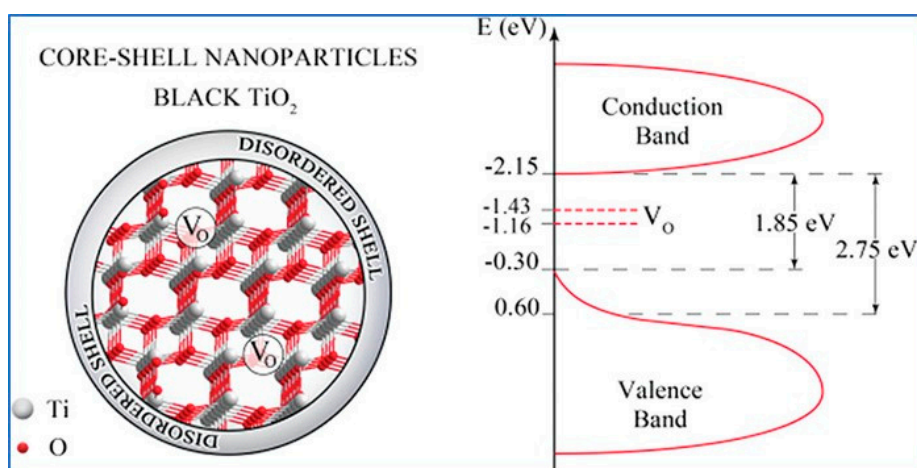


**Figure 3.** The density of states structure of black TiO$_2$ NPs with a crystalline and defective core, and a disordered shell [72].

### 3.2. Semiconductor-Based Heterojunctions

Semiconductor-mediated photocatalysis suffers from the drawbacks of short photogenerated electron–hole pair lifetime and the limited visible light absorption. Fabricating semiconductor heterojunctions has been one of the most widely used strategies over the past decade [77]. In general, the sensitivity range of PEC sensors is strongly dependent on the charge transfer of photoactive materials, which benefits from the high carrier density [78]. The formation of semiconductor-based heterojunction materials allows for the incorporation of materials that can adjust the bandgap energy, increase the charge carrier density, and then further suppress the recombination of photogenerated electron–hole pairs and attain their purpose of improving optoelectronic conversion efficiency.

### 3.2.1. Semiconductor–Semiconductor Heterojunctions

The Bi-based semiconductors, such as $BiPO_4$ [79–82], $BiVO_4$ [83–85], $Bi_2WO_6$ [86–88], and $BiFeO_3$ [89,90], are linked with the Bi 6s and O 2p hybrid orbitals of the narrowed bandgap as well as the deep valance band, which have received extensive attention in the study of PEC because of their efficient visible light photocatalytic activity [91]. $Bi_2WO_6$, as the simplest member of the Aurivillius family of layered perovskites, possesses good photon absorptivity under visible light irradiation [92]. However, unfortunately, it suffers from rapid photorecombination of carriers in a single component system. Adhikari et al. designed $Bi_2S_3$-sensitized $Bi_2WO_6$ microstructures topotactically via the hydrothermal technique under a controlled hydrothermal atmosphere and synthesized different weight percentage $Bi_2S_3/Bi_2WO_6$ microstructures for the evaluation of ofloxacin photo-oxidation under visible light [93]. In Figure 4b, after $Bi_2S_3$ is introduced into the $Bi_2WO_6$, we observe that a wide absorption band has been formed in the visible light range. The calculated energy bandgap is estimated to be 2.12 eV for 10 wt% $Bi_2S_3/Bi_2WO_6$. As shown in Figure 4a, both $Bi_2S_3$ and $Bi_2WO_6$ are excited to form a photogenerated electron–hole pair under the light illumination. The photogenerated electron in $Bi_2S_3$ flows to the conduction band of $Bi_2WO_6$, associated with the migration of photogenerated holes in the valence band of $Bi_2WO_6$ to the valence band of $Bi_2S_3$ simultaneously. Due to the favorable band positions of $Bi_2S_3$ and $Bi_2WO_6$, the electron–hole recombination could be effectively separated, which is helpful to the high photocatalytic degradation of ofloxacin. Therefore, when ofloxacin is added in the system, competition between photogenerated electrons to flow through the system and oxidize ofloxacin occurs, causing the decreasing of the photocurrent. On the basis of the surface plasmon resonance effect of metallic Bi, Li et al. coupled Bi and CuS, a narrow bandgap semiconducting material, with $Bi_2WO_6$ to prepare the Bi-$CuS/Bi_2WO_6$ heterojunction with enhanced separation of photo-generated charge carriers, charge transfer, and absorption wavelengths under visible light [87]. Then, a sensitive label-free PEC sensor found on Bi-$CuS/Bi_2WO_6$ nanocomposite was fabricated for the determination of paracetamol (PA), which is a ubiquitous NSAID. When PA is put into the electrolyte, the isolated holes on $Bi_2WO_6$ VB enter CuS to oxidize PA and acquire electrons, thus continuously producing photoelectrons to enhance the photocurrent signals.
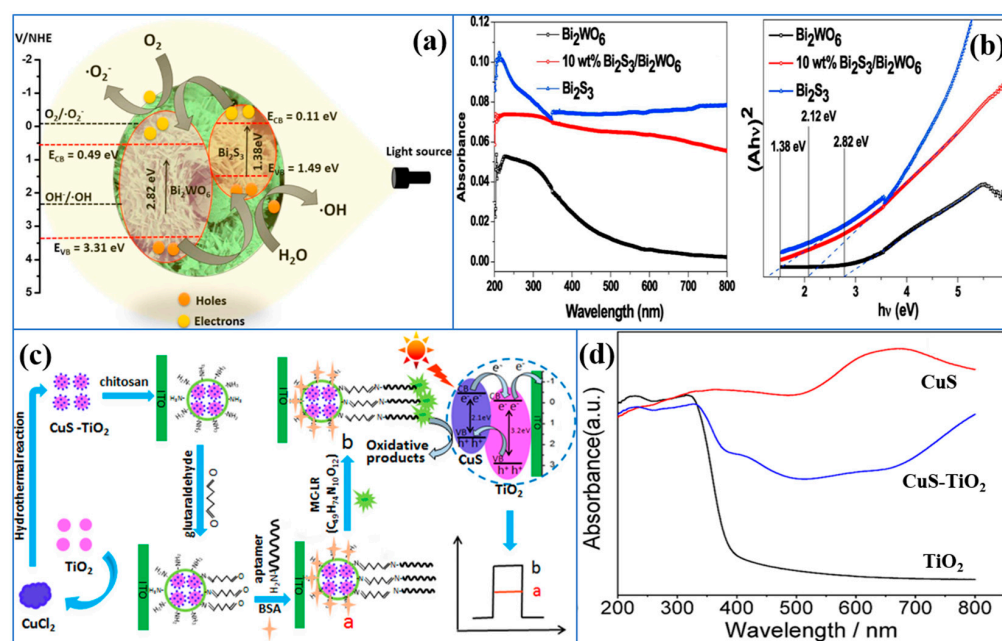
**Figure 4.** (**a**) The possible mechanism of photogenerated electron–hole transfer in $Bi_2S_3/Bi_2WO_6$ under light irradiation; (**b**) the UV–vis absorbance spectra and Tauc plot [93]. (**c**) Schematic diagram of the assembly and PEC mechanism of the fabricated aptasensor based on $CdS/TiO_2$ NRAs; (**d**) the diffuse reflectance spectroscopy of $TiO_2$ nanospheres, CuS NPs, and CuS–$TiO_2$ composite [6].

$TiO_2$ is the most widely used photoactive material, which has the advantages of strong photoactivity, good biocompatibility, low cost, and strong chemical stability in various environments [94,95]. Nevertheless, the light absorption in the visible region of $TiO_2$ is limited to a great extent because of the wide bandgap. $TiO_2$ can only absorb UV light ($\lambda < 400$ nm), which can kill biomolecules [96]. Therefore, the modification of $TiO_2$ with narrow-bandgap semiconductors is crucial for the PEC biosensing applications to not only enhance its absorption in the visible range but also to improve the lifetime of charge carriers. CdS, CuS, $MoS_2$, and $Ag_3VO_4$ are sensitive to the visible light excitation due to their narrow bandgap, about 2.27 eV, 2.1 eV, 1.9 eV, and 2.2 eV, respectively [73,97–99]. Wei et al. fabricated an ultrasensitive PEC immunoassay for the detection of MC–LR based on a sensitive PEC material of $CdS/TiO_2$ nanorod arrays ($CdS/TiO_2$ NRAs) to immobilize antigens [100]. The photogenerated holes of CdS NPs help to weaken the self-oxidation, limit the recombination of electron–hole pairs, as well as broaden the light absorption of $TiO_2$ NRAs then immobilize antigens as a visible light-driven material. The photocurrent values of the proposed immunosensor are linear from 0.005 to 500 µg $L^{-1}$ concentration of MC–LR, and the limit of detection is 0.001 µg $L^{-1}$. Tang et al. prepared a CuS–$TiO_2$ heterojunction composite via dispersedly depositing CuS NPs on $TiO_2$ nanospheres' surface, and they then constructed a PEC aptasensor for sensitive detection of MC–LR in an aquatic environment with a detection limit of $2.0 \times 10^{-5}$ nM and good stability, of whose initial value the photocurrent response at the PEC aptasensor retained ~91.8% after 10 days' storage in 4°C refrigerator (Figure 4c) [6]. As shown in Figure 4d, the absorption edge of CuS–$TiO_2$ heterojunction composite (~504 nm) is much longer than that of pure $TiO_2$ (~388.5 nm). The intensified visible light absorption works together with the improved separation of photogenerated charges and the reduced self-aggregation of CuS nanoparticles to obtain the superior analytical performance for MC–LR. Fan et al. developed a highly sensitive atrazine PEC aptasensor by exploring $TiO_2$ nanotubes decorated with $MoS_2$ quantum dots ($MoS_2$ QDs/$TiO_2$ NTs) as a photoelectrode [47]. Because the visible light absorption range of $TiO_2$ was effectively extended from UV to visible light by $MoS_2$ QDs, the bioactivity of the photoelectrode was well maintained. Therefore, the photoelectrode exhibits high binding capacity of aptamer molecules to targets, which helped the designed atrazine PEC

aptasensor achieve high sensitivity and specificity. Zhang et al. obtained a heterojunction of $Ag_3VO_4$ nanoparticles-deposited $TiO_2$ nanotube arrays (TNTAs) on a Ti foil electrode, which cooperated with oxygen vacancies of TNTAs caused by the electrochemical reduction treatment to greatly improve the visible light absorption of TNTAs, as well as the charge separation of TNTAs [73].

In addition, other new heterojunctions have also been reported as photosensitive material for the construction of PEC sensors for the analysis of toxins and abused drugs in the environment, such as the $CuCo_2O_4$@CoO core–shell hybrid rod for selectively sensing diclofenac [37], ZnPc/CN (zinc phthalocyanine/graphitic nitride) nanocomposite for preparing sulfadimethoxine aptasensor [101], hollow ZnS–CdS nanocage-based molecularly imprinted (ZnS–CdS/rMIP) PEC sensor for sensitive measurement of oxytetracycline [54], CdS nanorod arrays (CdS NRs)/$Ag_2S$ on FTO for PEC immunoassay of ochratoxins, and so on. The report results show that the semiconductor–semiconductor heterojunctions usually exhibit significantly improved photocurrent response compared with the pure semiconductor, which could help to increase the analytical performance of the PEC sensors remarkably.

### 3.2.2. Semiconductor–Carbon Heterojunctions

Carbon materials, such as graphene, reduced graphene oxide (rGO), graphene quantum dots (GQDs), graphite-phase carbon nitride (g-$C_3N_4$), carbon nanotubes (CNTs), and so on, all show the inherent advantages of strong chemical stability, good biocompatibility, low toxicity, superior electron mobility, and high specific surface area [30,102]. Therefore, they are usually combined with other semiconductor materials by forming nanohybrids to fabricate high performance PEC sensors [103,104]. The dramatic analytical performances of the PEC sensors are achieved in the following ways: the adsorption of more electroactive species, shortening charge transport time and distance, acceleration of the transfer of photogenerated electrons, and suppression the recombination of charge carriers.

Graphene [105], N-doped graphene [3,48,78], and reduced graphene oxide (rGO) [106–108] are the most common carbon materials used to design semiconductor–carbon heterojunctions in PEC sensors. Because of the non-photoactivity and zero bandgap, graphene was usually employed as a carrier or electron transfer promoter for fabricating PEC sensors [109–112]. Yan et al. proposed a novel cathodic "signal-off" strategy for oxytetracycline PEC aptasensing based on BiOI–graphene nanocomposite [113]. In this sensor, p-type semiconductor BiOI was used as photoactive species, while doping BiOI with a certain amount of graphene can not only improve the absorption in the visible light region but also facilitate the electron transfer of the photoanode. Except pure graphene, N-doped graphene is also used in the PEC field according to the increased bandgap of graphene with the doped N element [114,115]. Zhang et al. designed a novel visible light-driven self-powered PEC aptasensor for MC–LR detection based on 3D N-doped graphene hydrogel/hematite nanocomposites (NGH/$Fe_2O_3$), as shown in Figure 5a [78]. Three-dimensional NGH could trap the holes to suppress the recombination, thus promoting the transmission of photoinduced electrons and increasing the conductivity. Therefore, the coupling NGH with $Fe_2O_3$ could generate a Schottky junction that could promote the separation of charges and increase the performance of the aptasensor with a wide linear range of 1 pM to 5 nM. Ge et al. synthesized $Bi_2MoO_6$ nanoparticles-anchored boron and nitrogen co-doped graphene (BNG) nanosheets nanocomposites with oxygen vacancy [48]. The incorporation of BNG nanosheets increased the oxygen vacancies, broadened the light adsorption range, and accelerated the charge transfer. So, a highly efficient PEC aptasensor for sensitive analysis of lincomycin was constructed based on the prepared $Bi_2MoO_6$/BNG photoactive nanocomposite. In addition to graphene and doped graphene, rGO has also been applied to PEC sensing for its improved water dispersibility and chemical reactivity. However, rGO is a p-type semiconductor with a narrow bandgap and relatively poor conductivity, so rGO is frequently coupled with other semiconductor materials in PEC sensing field [116,117]. Lu et al. developed a visible light-driven PEC aptasensor for MC–LR based on rGO/Ti–Fe–

O nanotubes (NTs) [107]. It benefited from the large π-conjugated structure and unique electrical conductivity of rGO which endows a superhigh carrier migration rate. Therefore, the photo generated e⁻ can transfer to the surface of rGO rapidly, which effectively promotes the separation of photo-generated $e^-$-$h^+$ (as shown in Figure 5b). The fabricated aptasensor exhibits outstanding determination performance for MC–LR with a detection limitation of 5 fM.

Besides graphene-class materials, other carbon materials [38–40,118,119] are also used to synthesize semiconductor–carbon heterojunctions as photo-responsive materials for constructing PEC sensors. Liu et al. developed a MC–LR PEC sensor on a surface molecular-imprinted $TiO_2$-coated multiwalled carbon nanotubes (MI–$TiO_2$@CNTs) hybrid heterojunction nanostructure [119]. The sensor displayed a superior photocurrent response sensitivity and a wide linear range from 1.0 pM to 3.0 nM, which was mainly attributed to the high specific surface area and excellent photoelectric activity of the $TiO_2$@CNTs heterojunction nanostructure. As shown in Figure 5c, $TiO_2$ incurred charge separation under illumination, resulting in $e^-$-$h^+$. When $TiO_2$ NPs chemically bonded to the surface of CNTs, the electrons transferred from the CB of $TiO_2$ to the surface of CNTs due to their unique electrical conductivity and high electron storage performance. Therefore, the residual holes in $TiO_2$ VB could react with MC–LR that was absorbed on the electrode with MI recognition to produce an increased oxidation current. Gao et al. employed an electrophoretic deposition strategy to successfully fabricate a thin-film PEC sensor of functionalized N-doped graphene quantum dots embedded in BiOBr nanosheets that were loaded on ITO substrate (F-NGQDs/BiOBr/ITO) for paracetamol (PA) [38]. It was found that the thin film with NGQDs/BiOBr heterojunction showed enhanced charge transfer and absorption wavelengths under visible light, thus yielding an increase in the observed photocurrent. As shown in Figure 5d, the VB and CB positions of NGQDs are higher than those of BiOBr. The NGQDs are excited and undergo charge separation to generate $e^-$-$h^+$. Since BiOBr has different CB energy levels, photogenerated electrons are rapidly transferred to BiOBr, and then the separated holes on the VB of BiOBr can enter NCQDs and further oxidize PA to obtain electrons, thereby continuing to produce photoelectrons. Li et al. fabricated a novel bismuth vanadate/two-dimensional carbon nitride/deoxyribonucleic acid (BiVO₄/2D-C₃N₄/DNA) MC–LR aptamer PEC sensor with a detection sensitivity range of $5 \times 10^{-7}$ to 10 µg L$^{-1}$ [120]. The photogenerated charge transport process schematic diagram is shown in Figure 5e. 2D-C₃N₄ plays a key role in multifunctional interface reconciliation. To be specific, 2D-C₃N₄ not only serves as a photogenerated hole-oriented transfer medium from the BiVO₄ photoanode to the detective target; it also fixes the DNA aptamer parallelly via the π–π bond to shorten the hole transfer distance from the semiconductor to the target.
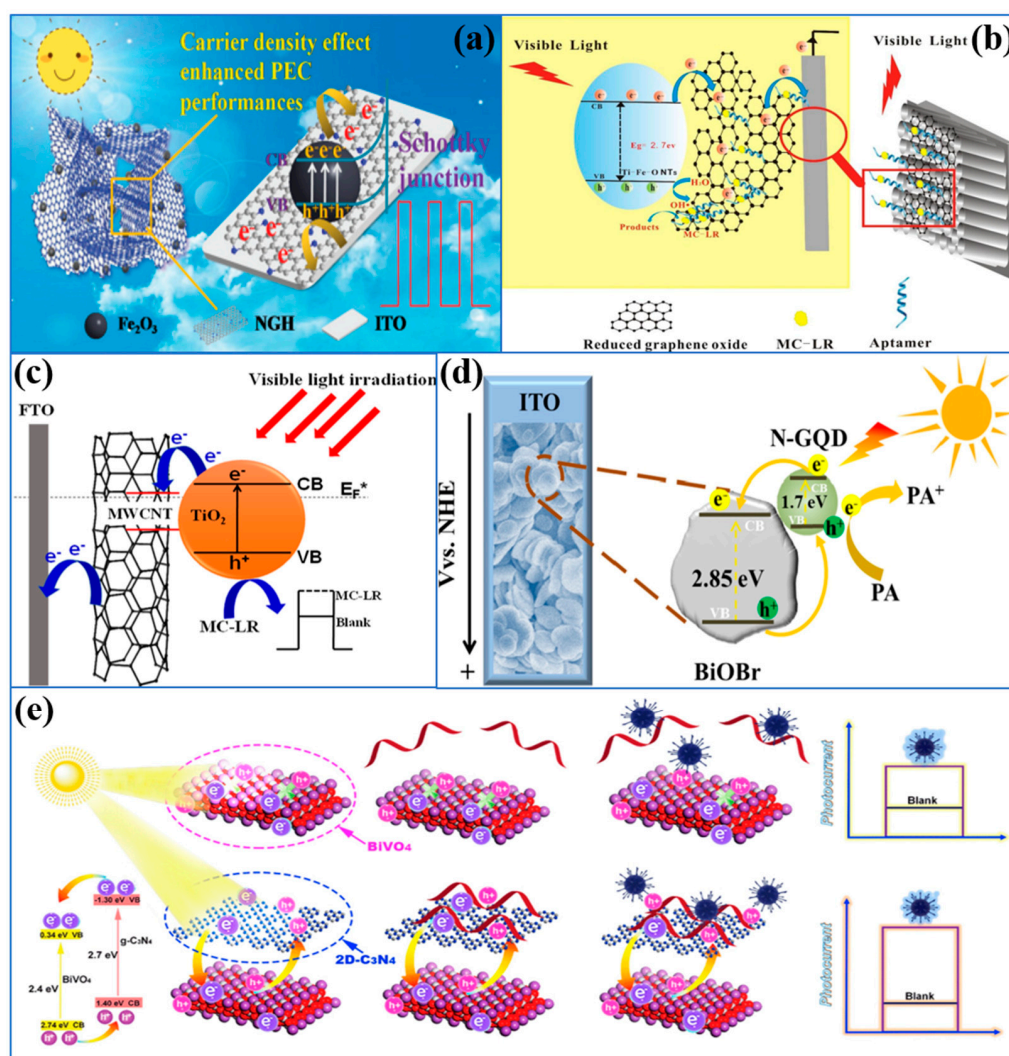
**Figure 5.** (**a**) and (**b**) Mechanism diagram of the MC–LR aptasensors based on NGH/Fe$_2$O$_3$ Schottky junctions [78] and rGO/Ti–Fe–O NTs [107], respectively. (**c**) Photoexcitation and electron-charge transfer process of the MI–TiO$_2$@CNTs/FTO [119]. (**d**) Electron-transfer mechanism of PA PEC sensor based on F-NGQDs/BiOBr/ITO electrode [38]. (**e**) Schematic of photogenerated charge transport process on BiVO$_4$/2D-C$_3$N$_4$/DNA aptamer PEC sensor [120].

### 3.2.3. Semiconductor–Metal Heterojunctions

The surface plasmon resonance (SPR) effect is an optical near-field effect on the localized surface of noble metal nanoparticles (e.g., Au, Ag, and Pd), resulting in enhanced local electromagnetic fields [121]. Thanks to this effect, the light absorption and photoelectric conversion efficiency of semiconductors can be greatly improved according to the excellent electron mediators of the noble metal nanoparticles through the rapid separation and transportation of photogenerated e$^-$-h$^+$ pairs at the semiconductor/metal interface [122]. Au NPs are the most commonly used noble metal [123,124]. Xu et al. constructed a facile and sensitive PEC sensing platform based on plasmonic Au/graphitic carbon nitride composites (Au/g-C$_3$N$_4$) for the detection of 4-chlorophenol (4-CP) [125]. As shown in Figure 6a, upon the illumination on the surface of Au/g-C$_3$N$_4$ composites, the photogenerated electrons of g-C$_3$N$_4$ can be quickly injected into Au. Due to the SPR effect of Au NPs, the interaction between Au NPs and incident light can generate a strong local electromagnetic field that induces plasmon oscillation on the local surface of Au NPs. Therefore, the photogenerated electrons are retained on the surface of Au NPs, which contributes to the effective separation of photogenerated e$^-$-h$^+$. At last, large number of electrons accumulating on the CB of

g-C$_3$N$_4$ and on the surface of Au NPs can flow to the external circuit via the ITO substrate, resulting a significant enhancement in the photocurrent density. Upon 4-CP introduction, holes in the g-C$_3$N$_4$ VB can be sacrificed by 4-CP, which suppresses the e$^-$-h$^+$ recombination then further enhances the photocurrent density. Employing ZnCuInSe (Zn-doped CuInSe$_2$ quantum dots)/Au/TiO$_2$ nanowires sandwich structure, Geng et al. developed a facile PEC aptasensor for kanamycin detection with a linear response range from 0.2 to 250 nM [126]. The Au NPs, which were sandwiched between the TiO$_2$ nanowires and the ZnCuInSe QDs layer, play a dual role in enhancing the photocurrent, as shown in Figure 6b. One is to serve as a photosensitizer that extends the light absorption of the electrode to the visible range; the other is to act as an electron relay that promotes charge transfer between the TiO$_2$ nanowires and ZnCuInSe QDs. Zhang et al. fabricated an atrazine aptasensor based on a Au NPs-modified 3D-ordered microporous (3DOM) TiO$_2$ nanostructure frame with high sensitivity, selectivity, and stability [127]. The fabricated PEC aptasensor exhibits the detection limit of 0.167 ng/L, outstanding anti-interference ability in 100-fold concentration of other endocrine disrupting compounds, and stable photocurrent response after over 2000 s visible light illumination. As shown in Figure 6c, under the visible light illumination, the photogenerated electrons are excited to the CB of 3DOM and the holes left. Au NPs can also produce hot electrons and holes via the SPR effect. According to the energy level of hot electrons and hot holes of Au NPs, as well as the CB and VB of TiO$_2$, the hot electrons generated by Au NPs are easily transferred to the CB of TiO$_2$, and then both are transferred to the external circuit through the FTO to generate photocurrent. As a result, visible light absorption is effectively enhanced and the recombination of photogenerated carriers is efficiently decreased.

In addition to Au, Ag [128–130], Cu [131,132], Pd [133,134], Bi [135,136], Pt [137] are also applied to construct composites with semiconductors, which are used as the substrates for the PEC sensor. Wang et al. developed a 4-chlorophenol (4-CP) PEC sensor based on ternary composites of Ag NPs, graphitic carbon nitride (GCN), and carbon spheres (CS) (Ag/GCN/CS), which shows that an enhanced PEC response might be attributed to the synergistic effect between the SPR of Ag NPs and the electron-transfer behavior of CS [128]. The plausible PEC mechanism of the Ag/GCN/CS/ITO is discussed in two incident light spectral regions of 420–550 nm and 550–800 nm, considering the absorption edge of pure GCN (about 550 nm), as shown in Figure 6d. Under the illumination of 420–550 nm, Ag NPs, as electron sinks, can capture the electrons generated by the excited GCN, thereby inhibiting e$^-$-h$^+$ recombination. Meanwhile, in the wavelength range of 550–800 nm, a strong oscillation of electrons occurs on the surface of Ag NPs according to the SPR effect, resulting in the transfer of hot electrons from the surface of Ag NPs to the CB of GCN, which can effectively reduce the recombination rate of electrons and holes. Xu et al. prepared a nanocomposite of Bi-doped ultrathin polymeric carbon nitride (Bi/CV-PCN) with carbon vacancies (CVs), displaying high PEC activity and stability, to utilize as the photoactive material for fabricating an enrofloxacin (ENR) aptasensor. As shown in Figure 6e, the electrons in the VB of PCN are excited to the CVs under visible light irradiation, following further transition to the CB of PCN. Since the CB of PCN is more negative than the Fermi level of Bi, the electrons are subsequently transferred from PCN to metal Bi. The addition of Bi metal plays two roles in improving the light trapping ability of PCN, besides accelerating the separation of photogenerated charge carries according to the built-in electric field originating from the SPR effect of Bi. At last, the holes left in the VB of PCN directly oxidize the ENR to produce photocurrent. The synergistic effect of the CVs that form an intermediate energy level, and the SPR effect of Bi, effectively boost the visible light harvesting ability and improve charge separation efficiency, finally resulting in a remarkable improvement on the PEC performance.
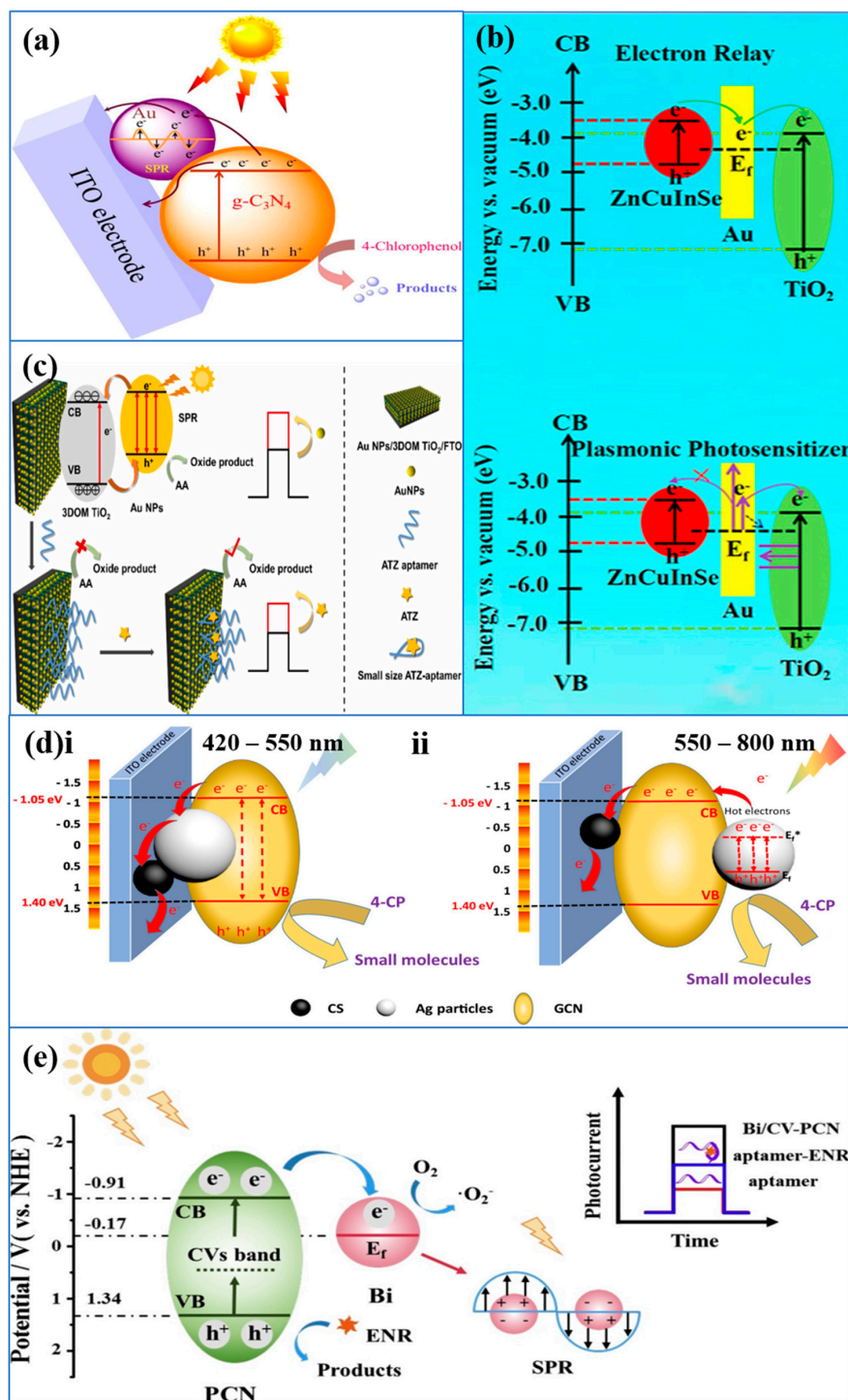
**Figure 6.** (**a**) Photocurrent generation mechanism schematic diagram of Au/g-C₃N₄/ITO electrode [125]. (**b**) Dual role of the Au nanoparticles in the ZnCuInSe/Au/TiO₂ sandwich structure serving as a plasmonic photosensitizer and an electron relay [126]. (**c**) The mechanism of atrazine PEC sensor based on Au NPs/3DOM TiO₂/FTO [127]. (**d**) The plausible PEC mechanism of the Ag/GCN/CS/ITO in different spectral regions of (i) 420–550 nm and (ii) 550–800 nm [128]. (**e**) Electron-transfer mechanism of ENR sensing based on the Bi/CV-PCN composite [136].

### 3.2.4. Multi-Component Heterojunctions

Considering the synergistic effect, multi-component heterojunctions composed of visible light active components and electron transfer systems are spatially integrated for

the purpose of simultaneously achieving an enhanced visible light response and transfer of charge carriers. Semiconductor, carbon material, and noble metal nanoparticles amount to a good combination, which effectively combines the light absorption and electron transfer ability and SPR effect [128]. Ouyang et al. designed a heterojunction based on coupling $CeO_2$ quantum dots (QDs) with graphitic carbon nitride (g-CN) and Au nanoparticles (ACG) for fabricating a self-powered PEC MC–LR aptasensor with a detection limit of 0.01 pM [40]. As shown in Figure 7a, because of the combination of $CeO_2$ QDs and the g-CN nanosheet into a highly dispersed nanocomposite, the matched band potentials and closely contacted interface between them can efficiently suppress the recombination of photo-generated electron–hole pairs and promote charge separation, which benefits the as-obtained PEC aptasensor to exhibit excellent analytical performances. The Au nanoparticles not only provide many binding sites for MC–LR aptamers through Au-S bond; they also greatly increase the light absorption capacity because of the SPR effect. Similarly, the $CoO/Au/g-C_3N_4$ Z-scheme heterojunction [138], Au nanoparticles, and graphene-doped CdS composite [139] were designed to fabricate the PEC sensor.

Semiconductorsand dye molecules-co-sensitized $TiO_2$ is also a good combination. The dye molecules can be adsorbed on the surface of semiconductors, increasing their photo response owing to the greater absorption of the light in the visible region [140]. Lima et al. used $TiO_2$ to co-sensitize with N-methylphenazonium methyl sulfate (PMS) and CdTe QDs; the composite was then immobilized in a Nafion film that severed as the photoelectroactive element for the development of a PEC sensor for the detection of tannic acid [141]. PMS was exploited as a co-modifier of the $TiO_2$, aimed to produce a stable materialthat photo-sensitive to visible LED light in this study. Sousa et al. fabricated a naringin PEC sensor on a zero-biased fluorine-doped tin oxide (FTO) electrode modified with CdS and chloro-protoporphyrin IX iron(III) (CPPI)-sensitized $TiO_2$, designated CPPI–$TiO_2$/CdS/FTO [142]. The proposed mechanism for the naringin PEC detection is shown in Figure 7b. The CPPI adsorbed on $TiO_2$ particles can absorb light to produce photoexcited states (CPPI*) then inject electrons into the conduction band of $TiO_2$, resulting, simultaneously, in an oxidized form of CPPI+. On the other hand, the CdS can also be excited by visible light to produce electrons and holes in the CB and VB, respectively. Therefore, the photoelectron at the CB of $TiO_2$ can react with the holes at the VB of CdS via a mean z-scheme. Eventually, the photoelectrons on the CB of CdS can be collected from the FTO electrode to generate an anodic photocurrent. In addition to the above-mentioned multi-component heterojunctions, other combinations have also been reported for the analysis of toxins and abused drugs in the environment, such as $CdS/Fe_2O_3$ co-sensitized $TiO_2$ nanorod arrays [143], $TiO_2$/CNTs/CdTeQDs [144], $In_2O_3-In_2S_3-Ti_3C_2$ composite [145], and so on.
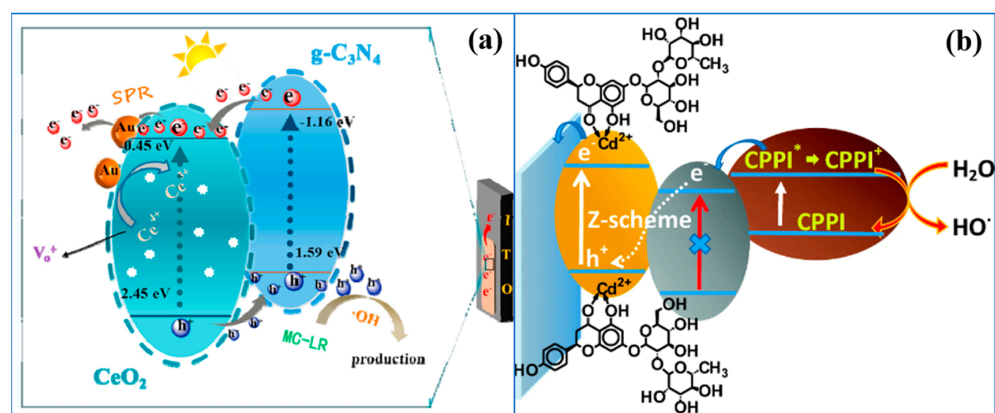


**Figure 7.** (**a**) The mechanism of MC–LR PEC aptasensor based on ACG heterostructure [40]. (**b**) Proposed mechanism for the naringin photoelectrochemical detection based on the CPPI–$TiO_2$/CdS platform. CPPI* means the photoexcited states of CPPI [142].

## 4. Summary and Outlook

Due to the high sensitivity and low cost of PEC sensors, numerous PEC sensors have been fabricated for the rapid and accurate monitoring of toxins and abused drugs in the environment. It was found that the photoelectric conversion efficiency was obviously improved via the innovative design and controllable preparation of photoactive materials. This review mainly summarizes the composition of the engineered photoactive materials, the sensing mechanisms, and actual applications of the fabricated PEC sensors.

Although great progress in the PEC sensing of toxins and abused drugs in the environment has been made by far, there is still plenty of room for development and further applications in the future. Firstly, multi-signal amplification strategies and multi-component heterojunctions are usually used to construct PEC sensors, which might increase the fabrication difficulty and cost, as well as reduce the stability of the PEC sensors. Therefore, it is of great importance to develop highly efficient signal amplification strategies and to prepare high-quality and environmentally friendly photoactive heterojunctions because employment of the often-used, traditional QDs (e.g., CdS) would lead to a second pollution. In addition, most of the reported PEC sensors are focused on the quantitative single-target analysis. A broad–specific PEC immunosensor was constructed for the simultaneous detection of ochratoxin A, ochratoxin B, and ochratoxin C because of the electronegativity of the chlorine atom that increases the antibody binding ability. Considering the difficulty of broad-spectrum antibodies, research can focus on developing an aptamer with multiple recognition sites for multiple-target detection simultaneously. Moreover, integrating PEC sensors with microfluidics and chips is also a good strategy by which to increase detection efficiency via multi-channel simultaneous detection. A microfluidic system with a paper working electrode combined with the PEC sensing technique is also an intelligent design that could facilitate miniaturization and assist integration into portable devices. Furthermore, qualitative detection of unknown toxins and abused drugs in the environment is also urgently needed. The designing of photoactive materials with specific sites and coupling PEC sensing with other methods, such as cyclic voltammetry (CV) and differential pulse voltammetry (DPV), have been reported as effective ways. However, a highly stable light source is usually required to excite the PEC sensors, which also greatly limits their practicality. Consequently, solar-powered and self-powered PEC sensors combined with energy conversion devices are being developed.

**Author Contributions:** Writing—original draft preparation, Y.M.; X.L.; Y.B. and L.N.; writing—review and editing, Y.M.; X.L.; Y.B. and L.N.; supervision, Y.B.; All authors have read and agreed to the published version of the manuscript.

**Institutional Review Board Statement:** Not applicable.

**Informed Consent Statement:** Not applicable.

**Conflicts of Interest:** The authors declare no conflict of interest.

## References

1. Munoz, M.; Cires, S.; de Pedro, Z.M.; Colina, J.A.; Velasquez-Figueroa, Y.; Carmona-Jimenez, J.; Caro-Borrero, A.; Salazar, A.; Fuster, M.C.S.; Contreras, D.; et al. Overview of toxic cyanobacteria and cyanotoxins in Ibero-American freshwaters: Challenges for risk management and opportunities for removal by advanced technologies. *Sci. Total Environ.* **2021**, *761*, 143197. [CrossRef]
2. Chen, L.K.; Guo, C.S.; Sun, Z.Y.; Xu, J. Occurrence, bioaccumulation and toxicological effect of drugs of abuse in aquatic ecosystem: A review. *Environ. Res.* **2021**, *200*, 111362. [CrossRef]
3. Du, X.; Jiang, D.; Li, H.; Hao, N.; You, T.; Wang, K. An intriguing signal-off responsive photoelectrochemical aptasensor for ultrasensitive detection of microcystin-LR and its mechanism study. *Sens. Actuator B-Chem.* **2018**, *259*, 316–324. [CrossRef]

4. Xu, J.Y.; Zhang, W.Y.; Zhong, S.Z.; Xie, X.X.; Che, H.M.; Si, W.R.; Tuo, X.; Xu, D.X.; Zhao, S.J. Microcystin-leucine-arginine affects brain gene expression programs and behaviors of offspring through paternal epigenetic information. *Sci. Total Environ.* **2023**, *857*, 159032. [CrossRef]

5. Guo, X.; Meng, R.Y.; Liu, J.J.; Zhang, S.Y.; Liu, H.H.; Du, X.D.; Zhang, H.Z.; Li, Y.S. Microcystin leucine arginine induces human sperm damage: Involvement of the $Ca^{2+}$/CaMKKβ/AMPK pathway. *Ecotoxicol. Environ. Saf.* **2023**, *256*, 114845. [CrossRef]

6. Tang, Y.; Chai, Y.; Liu, X.; Li, L.; Yang, L.; Liu, P.; Zhou, Y.; Ju, H.; Cheng, Y. A photoelectrochemical aptasensor constructed with core-shell $CuS$-$TiO_2$ heterostructure for detection of microcystin-LR. *Biosens. Bioelectron.* **2018**, *117*, 224–231. [CrossRef] [PubMed]

7. Krishnan, R.Y.; Manikandan, S.; Subbaiya, R.; Biruntha, M.; Balachandar, R.; Karmegam, N. Origin, transport and ecological risk assessment of illicit drugs in the environment—A review. *Chemosphere* **2023**, *311*, 137091. [CrossRef]

8. Metcalfe, C.D.; Bayen, S.; Desrosiers, M.; Munoz, G.; Sauve, S.; Yargeau, V. An introduction to the sources, fate, occurrence and effects of endocrine disrupting chemicals released into the environment. *Environ. Res.* **2022**, *207*, 112658. [CrossRef] [PubMed]

9. Fent, K.; Weston, A.A.; Caminada, D. Ecotoxicology of human pharmaceuticals. *Aquat. Toxicol.* **2006**, *76*, 122–159. [CrossRef]

10. Michalaki, A.; Grintzalis, K. Acute and Transgenerational Effects of Non-Steroidal Anti-Inflammatory Drugs on Daphnia magna. *Toxics* **2023**, *11*, 320. [CrossRef]

11. Parolini, M. Toxicity of the Non-Steroidal Anti-Inflammatory Drugs (NSAIDs) acetylsalicylic acid, paracetamol, diclofenac, ibuprofen and naproxen towards freshwater invertebrates: A review. *Sci. Total Environ.* **2020**, *740*, 140043. [CrossRef]

12. Patel, M.; Kumar, R.; Kishor, K.; Mlsna, T.; Pittman, C.U.; Mohan, D. Pharmaceuticals of Emerging Concern in Aquatic Systems: Chemistry, Occurrence, Effects, and Removal Methods. *Chem. Rev.* **2019**, *119*, 3510–3673. [CrossRef]

13. Marmon, P.; Owen, S.F.; Margiotta-Casaluci, L. Pharmacology-informed prediction of the risk posed to fish by mixtures of non-steroidal anti-inflammatory drugs (NSAIDs) in the environment. *Environ. Int.* **2021**, *146*, 106222. [CrossRef] [PubMed]

14. Zastepa, A.; Pick, F.R.; Blais, J.M.; Saleem, A. Analysis of intracellular and extracellular microcystin variants in sediments and pore waters by accelerated solvent extraction and high performance liquid chromatography-tandem mass spectrometry. *Anal. Chim. Acta* **2015**, *872*, 26–34. [CrossRef] [PubMed]

15. Fresco-Cala, B.; Gálvez-Vergara, A.; Cárdenas, S. Preparation, characterization and evaluation of hydrophilic polymers containing magnetic nanoparticles and amine-modified carbon nanotubes for the determination of anti-inflammatory drugs in urine samples. *Talanta* **2020**, *218*, 121124. [CrossRef]

16. Vardali, S.; Papadouli, C.; Rigos, G.; Nengas, I.; Panagiotaki, P.; Golomazou, E. Recent Advances in Mycotoxin Determination in Fish Feed Ingredients. *Molecules* **2023**, *28*, 2519. [CrossRef] [PubMed]

17. Foss, A.J.; Aubel, M.T. Using the MMPB technique to confirm microcystin concentrations in water measured by ELISA and HPLC (UV, MS, MS/MS). *Toxicon* **2015**, *104*, 91–101. [CrossRef]

18. Liu, J.; Xing, Y.; Lin, Y.; Xie, Y.; Zhou, X. Effect of pretreatment approach on the ELISA-based detection of cyanotoxins in water: Analysis and application. *Sci. Total Environ.* **2023**, *871*, 161988. [CrossRef]

19. Garg, K.; Villavicencio-Aguilar, F.; Solano-Rivera, F.; Gilbert, L. Analytical Validation of a Direct Competitive ELISA for Multiple Mycotoxin Detection in Human Serum. *Toxins* **2022**, *14*, 727. [CrossRef]

20. Abdelwahab, N.S.; Abdelrahman, M.M. Simultaneous Determination of Methocarbamol and Ibuprofen by First Derivative Synchronous Fluorescence Spectroscopic Method in Their Binary Mixture and Spiked Human Plasma. *J. Fluoresc.* **2014**, *24*, 129–135. [CrossRef]

21. Pouyanfar, N.; Harofte, S.Z.; Soltani, M.; Siavashy, S.; Asadian, E.; Ghorbani-Bidkorbeh, F.; Kecili, R.; Hussain, C.M. Artificial intelligence-based microfluidic platforms for the sensitive detection of environmental pollutants: Recent advances and prospects. *Trends Environ. Anal. Chem.* **2022**, *34*, e00160. [CrossRef]

22. Zhao, W.-W.; Xu, J.-J.; Chen, H.-Y. Photoelectrochemical bioanalysis: The state of the art. *Chem. Soc. Rev.* **2015**, *44*, 729–741. [CrossRef] [PubMed]

23. Ma, X.; Kang, J.; Wu, Y.; Pang, C.; Li, S.; Li, J.; Xiong, Y.; Luo, J.; Wang, M.; Xu, Z. Recent advances in metal/covalent organic framework-based materials for photoelectrochemical sensing applications. *Trac-Trends Anal. Chem.* **2022**, *157*, 116793. [CrossRef]

24. Bilge, S.; Sınağ, A. Current trends and strategies in the development of green MXene-based photoelectrochemical sensing application. *Trac-Trends Anal. Chem.* **2023**, *163*, 117059. [CrossRef]

25. Qureshi, A.; Shaikh, T.; Niazi, J.H. Semiconductor quantum dots in photoelectrochemical sensors from fabrication to biosensing applications. *Analyst* **2023**, *148*, 1633–1652. [CrossRef]

26. Wang, H.-Y.; Xu, Y.-T.; Wang, B.; Yu, S.-Y.; Shi, X.-M.; Zhao, W.-W.; Jiang, D.; Chen, H.-Y.; Xu, J.-J. A Photoelectrochemical Nanoreactor for Single-Cell Sampling and Near Zero-Background Faradaic Detection of Intracellular microRNA. *Angew. Chem. Int. Ed.* **2022**, *61*, e202212752.

27. Li, C.-J.; Hu, J.; Gao, G.; Chen, J.-H.; Wang, C.-S.; Zhou, H.; Chen, G.; Qu, P.; Lin, P.; Zhao, W.-W. Biomolecules-Incorporated Metal-Organic Frameworks Gated Light-Sensitive Organic Photoelectrochemical Transistor for Biodetection. *Adv. Funct. Mater.* **2023**, *33*, 2211277. [CrossRef]

28. Shi, L.; Yin, Y.; Zhang, L.-C.; Wang, S.; Sillanpää, M.; Sun, H. Design and engineering heterojunctions for the photoelectrochemical monitoring of environmental pollutants: A review. *Appl. Catal. B* **2019**, *248*, 405–422. [CrossRef]

29. Yang, L.; Liu, X.; Li, L.; Zhang, S.; Zheng, H.; Tang, Y.; Ju, H. A visible light photoelectrochemical sandwich aptasensor for adenosine triphosphate based on $MgIn_2S_4$-$TiO_2$ nanoarray heterojunction. *Biosens. Bioelectron.* **2019**, *142*, 111487. [CrossRef]

30. Wang, H.; Xu, Y.; Xu, D.; Chen, L.; Qiu, X.; Zhu, Y. Graphitic Carbon Nitride for Photoelectrochemical Detection of Environmental Pollutants. *ACS EST Engg.* **2022**, *2*, 140–157. [CrossRef]

31. Hao, N.; Zhang, Y.; Zhong, H.; Zhou, Z.; Hua, R.; Qian, J.; Liu, Q.; Li, H.; Wang, K. Design of a Dual Channel Self-Reference Photoelectrochemical Biosensor. *Anal. Chem.* **2017**, *89*, 10133–10136. [CrossRef] [PubMed]

32. Zhou, Q.; Tang, D. Recent advances in photoelectrochemical biosensors for analysis of mycotoxins in food. *Trac-Trends Anal. Chem.* **2020**, *124*, 115814. [CrossRef]

33. Peng, B.; Tang, L.; Zeng, G.M.; Zhou, Y.Y.; Zhang, Y.; Long, B.Q.; Fang, S.Y.; Chen, S.; Yu, J.F. Current Progress in Aptasensors for Heavy Metal Ions Based on Photoelectrochemical Method: A Review. *Curr. Anal. Chem.* **2018**, *14*, 4–12. [CrossRef]

34. Wang, H.; Zhang, B.; Tang, Y.; Wang, C.; Zhao, F.; Zeng, B. Recent advances in bismuth oxyhalide-based functional materials for photoelectrochemical sensing. *Trac-Trends Anal. Chem.* **2020**, *131*, 116020. [CrossRef]

35. Chen, W.F.; Liu, S.Y.; Fu, Y.K.; Yan, H.C.; Qin, L.; Lai, C.; Zhang, C.; Ye, H.Y.; Chen, W.J.; Qin, F.Z.; et al. Recent advances in photoelectrocatalysis for environmental applications: Sensing, pollutants removal and microbial inactivation. *Coord. Chem. Rev.* **2022**, *454*, 214341. [CrossRef]

36. Shi, Y.T.; Zou, Y.T.; Khan, M.S.; Zhang, M.G.; Yan, J.; Zheng, X.H.; Wang, W.Q.; Xie, Z.G. Metal-organic framework-derived photoelectrochemical sensors: Structural design and biosensing technology. *J. Mater. Chem. C* **2023**, *11*, 3692–3709. [CrossRef]

37. Wang, Q.; Jiang, M.; Zhang, L. Label-free and visible-light driven photoelectrochemical sensor with $CuCo_2O_4$@CoO Core-shell hybrid rod as photoanode for selective sensing diclofenac. *Electrochim. Acta* **2021**, *397*, 139239. [CrossRef]

38. Gao, K.; Bai, X.; Zhang, Y.; Ji, Y. N–doped graphene quantum dots embedded in BiOBr nanosheets as hybrid thin film electrode for quantitative photoelectrochemical detection paracetamol. *Electrochim. Acta* **2019**, *318*, 422–429. [CrossRef]

39. Shi, T.; Wen, Z.; Ding, L.; Liu, Q.; Guo, Y.; Ding, C.; Wang, K. Visible/near-infrared light response VOPc/carbon nitride nanocomposites: VOPc sensitizing carbon nitride to improve photo-to-current conversion efficiency for fabricating photoelectrochemical diclofenac aptasensor. *Sens. Actuator B-Chem.* **2019**, *299*, 126834. [CrossRef]

40. Ouyang, X.; Tang, L.; Feng, C.; Peng, B.; Liu, Y.; Ren, X.; Zhu, X.; Tan, J.; Hu, X. $Au/CeO_2/g$-$C_3N_4$ heterostructures: Designing a self-powered aptasensor for ultrasensitive detection of Microcystin-LR by density functional theory. *Biosens. Bioelectron.* **2020**, *164*, 112328. [CrossRef] [PubMed]

41. Bostan, H.B.; Taghdisi, S.M.; Bowen, J.L.; Demertzis, N.; Rezaee, R.; Panahi, Y.; Tsatsakis, A.M.; Karimi, G. Determination of microcystin-LR, employing aptasensors. *Biosens. Bioelectron.* **2018**, *119*, 110–118. [CrossRef]

42. Fan, L.; Xiao, G.; Wang, M.; Zhao, S.; Yang, Q.; Cheng, L.; Huang, J.J.; Yue, Z. Ultrasensitive photoelectrochemical microcystin-LR immunosensor using carboxyl-functionalized graphene oxide enhanced gold nanoclusters for signal amplification. *Anal. Chim. Acta* **2021**, *1185*, 339078. [CrossRef] [PubMed]

43. Qileng, A.; Wei, J.; Lu, N.; Liu, W.; Cai, Y.; Chen, M.; Lei, H.; Liu, Y. Broad-specificity photoelectrochemical immunoassay for the simultaneous detection of ochratoxin A, ochratoxin B and ochratoxin C. *Biosens. Bioelectron.* **2018**, *106*, 219–226. [CrossRef]

44. Bai, X.Y.; Gao, W.K.; Zhou, C.H.; Zhao, D.Y.; Zhang, Y.; Jia, N.Q. Photoelectrochemical determination of diclofenac using oriented single-crystalline $TiO_2$ nanoarray modified with molecularly imprinted polypyrrole. *Microchim. Acta* **2022**, *189*, 90. [CrossRef]

45. Chen, J.; Gao, P.; Wang, H.; Han, L.; Zhang, Y.; Wang, P.; Jia, N. A $PPy/Cu_2O$ molecularly imprinted composite film-based visible light-responsive photoelectrochemical sensor for microcystin-LR. *J. Mater. Chem.* **2018**, *6*, 3937–3944. [CrossRef]

46. Wang, H.; Liang, D.; Xu, Y.; Liang, X.; Qiu, X.; Lin, Z. A highly efficient photoelectrochemical sensor for detection of chlorpyrifos based on 2D/2D β-Bi2O3/g-C3N4 heterojunctions. *Environ. Sci.-Nano* **2021**, *8*, 773–783. [CrossRef]

47. Fan, L.; Zhang, C.; Liang, G.; Yan, W.; Guo, Y.; Bi, Y.; Dong, C. Highly sensitive photoelectrochemical aptasensor based on $MoS_2$ quantum dots/$TiO_2$ nanotubes for detection of atrazine. *Sens. Actuator B-Chem.* **2021**, *334*, 129652. [CrossRef]

48. Ge, L.; Liu, Q.; Jiang, D.; Ding, L.; Wen, Z.; Guo, Y.; Ding, C.; Wang, K. Oxygen vacancy enhanced photoelectrochemical performance of $Bi_2MoO_6$/B, N co-doped graphene for fabricating lincomycin aptasensor. *Biosens. Bioelectron.* **2019**, *135*, 145–152. [CrossRef]

49. Chen, K.; Liu, M.; Zhao, G.; Shi, H.; Fan, L.; Zhao, S. Fabrication of a Novel and Simple Microcystin-LR Photoelectrochemical Sensor with High Sensitivity and Selectivity. *Environ. Sci. Technol.* **2012**, *46*, 11955–11961. [CrossRef]

50. Zhang, Z.; Huang, L.; Sheng, S.; Jiang, C.; Wang, Y. MIL-125(Ti)-derived COOH functionalized $TiO_2$ grafted molecularly imprinted polymers for photoelectrochemical sensing of ofloxacin. *Sens. Actuator B-Chem.* **2021**, *343*, 130119. [CrossRef]

51. Zu, M.; Zhou, X.; Zhang, S.; Qian, S.; Li, D.-S.; Liu, X.; Zhang, S. Sustainable engineering of $TiO_2$-based advanced oxidation technologies: From photocatalyst to application devices. *J. Mater. Sci. Technol.* **2021**, *78*, 202–222. [CrossRef]

52. Liu, Y.; Gan, X.; Zhou, B.; Xiong, B.; Li, J.; Dong, C.; Bai, J.; Cai, W. Photoelectrocatalytic degradation of tetracycline by highly effective $TiO_2$ nanopore arrays electrode. *J. Hazard. Mater.* **2009**, *171*, 678–683. [CrossRef] [PubMed]

53. Shamraiz, U.; Hussain, R.A.; Badshah, A. Fabrication and applications of copper sulfide (CuS) nanostructures. *J. Solid State Chem.* **2016**, *238*, 25–40. [CrossRef]

54. Bai, X.; Zhang, Y.; Gao, W.; Zhao, D.; Yang, D.; Jia, N. Hollow ZnS–CdS nanocage based photoelectrochemical sensor combined with molecularly imprinting technology for sensitive detection of oxytetracycline. *Biosens. Bioelectron.* **2020**, *168*, 112522. [CrossRef] [PubMed]

55. Yan, P.; Jiang, D.; Li, H.; Bao, J.; Xu, L.; Qian, J.; Chen, C.; Xia, J. $BiPO_4$ nanocrystal/BiOCl nanosheet heterojunction as the basis for a photoelectrochemical 4-chlorophenol sensor. *Sens. Actuator B-Chem.* **2019**, *279*, 466–475. [CrossRef]

56. Yu, S.-Y.; Zhang, L.; Zhu, L.-B.; Gao, Y.; Fan, G.-C.; Han, D.-M.; Chen, G.; Zhao, W.-W. Bismuth-containing semiconductors for photoelectrochemical sensing and biosensing. *Coord. Chem. Rev.* **2019**, *393*, 9–20. [CrossRef]

57. Zhou, Y.; Yin, H.; Ai, S. Recent advances and applications of Bi$_2$S$_3$-based composites in photoelectrochemical sensors and biosensors. *Trac-Trends Anal. Chem.* **2023**, *158*, 116876. [CrossRef]

58. Li, R.; Liu, Y.; Cheng, L.; Yang, C.; Zhang, J. Photoelectrochemical Aptasensing of Kanamycin Using Visible Light-Activated Carbon Nitride and Graphene Oxide Nanocomposites. *Anal. Chem.* **2014**, *86*, 9372–9375. [CrossRef]

59. Low, S.S.; Chen, Z.; Li, Y.; Lu, Y.; Liu, Q. Design principle in biosensing: Critical analysis based on graphitic carbon nitride (G-C$_3$N$_4$) photoelectrochemical biosensor. *Trac-Trends Anal. Chem.* **2021**, *145*, 116454. [CrossRef]

60. Li, Y.; Zhang, N.; Zhao, W.-W.; Jiang, D.-C.; Xu, J.-J.; Chen, H.-Y. Polymer Dots for Photoelectrochemical Bioanalysis. *Anal. Chem.* **2017**, *89*, 4945–4950. [CrossRef]

61. Wang, C.; Wang, H.; Zhang, M.; Zeng, B.; Zhao, F. Molecularly imprinted photoelectrochemical sensor for aflatoxin B1 detection based on organic/inorganic hybrid nanorod arrays. *Sens. Actuator B-Chem.* **2021**, *339*, 129900. [CrossRef]

62. Li, L.; Zhang, S.; Zhao, H. A low cost universal photoelectrochemical detector for organic compounds based on photoelectrocatalytic oxidation at a nanostructured TiO$_2$ photoanode. *J. Electroanal. Chem.* **2011**, *656*, 211–217. [CrossRef]

63. Özcan, L. Photoelectrochemical determination of paracetamol by using TiO$_2$ modified FTO electrodes. *Anal. Bioanal. Electrochem.* **2019**, *11*, 1117–1128.

64. Lin, Y.-M.; Tseng, Y.-H.; Huang, J.-H.; Chao, C.C.; Chen, C.-C.; Wang, I. Photocatalytic Activity for Degradation of Nitrogen Oxides over Visible Light Responsive Titania-Based Photocatalysts. *Environ. Sci. Technol.* **2006**, *40*, 1616–1621. [CrossRef] [PubMed]

65. Fan, D.; Wang, H.; Khan, M.S.; Bao, C.; Wang, H.; Wu, D.; Wei, Q.; Du, B. An ultrasensitive photoelectrochemical immunosensor for insulin detection based on BiOBr/Ag$_2$S composite by in-situ growth method with high visible-light activity. *Biosens. Bioelectron.* **2017**, *97*, 253–259. [CrossRef]

66. Chava, R.K.; Kang, M. Improving the photovoltaic conversion efficiency of ZnO based dye sensitized solar cells by indium doping. *J. Alloys Compd.* **2017**, *692*, 67–76. [CrossRef]

67. Chahrour, K.M.; Ooi, P.C.; Eid, A.M.; Nazeer, A.A.; Madkour, M.; Dee, C.F.; Wee, M.F.M.R.; Hamzah, A.A. Synergistic effect of bi-phased and self-doped Ti$^{3+}$ on anodic TiO$_2$ nanotubes photoelectrode for photoelectrochemical sensing. *J. Alloys Compd.* **2022**, *900*, 163496. [CrossRef]

68. Chen, L.-C.; Tu, Y.-J.; Wang, Y.-S.; Kan, R.-S.; Huang, C.-M. Characterization and photoreactivity of N-, S-, and C-doped ZnO under UV and visible light illumination. *J. Photochem. Photobiol. A* **2008**, *199*, 170–178. [CrossRef]

69. Wang, J.; Wang, X.; Yan, J.; Tan, Q.; Liang, G.; Qu, S.; Zhong, Z. Enhanced Photoelectrochemical Properties of Ti$^{3+}$ Self-Doped Branched TiO$_2$ Nanorod Arrays with Visible Light Absorption. *Material* **2018**, *11*, 1791. [CrossRef]

70. Li, H.; Qiao, Y.; Li, J.; Fang, H.; Fan, D.; Wang, W. A sensitive and label-free photoelectrochemical aptasensor using Co-doped ZnO diluted magnetic semiconductor nanoparticles. *Biosens. Bioelectron.* **2016**, *77*, 378–384. [CrossRef]

71. Zheng, L.; Zhang, H.; Won, M.; Kim, E.; Li, M.; Kim, J.S. Codoping g-C$_3$N$_4$ with boron and graphene quantum dots: Enhancement of charge transfer for ultrasensitive and selective photoelectrochemical detection of dopamine. *Biosens. Bioelectron.* **2023**, *224*, 115050. [CrossRef] [PubMed]

72. Naldoni, A.; Allieta, M.; Santangelo, S.; Marelli, M.; Fabbri, F.; Cappelli, S.; Bianchi, C.L.; Psaro, R.; Dal Santo, V. Effect of Nature and Location of Defects on Bandgap Narrowing in Black TiO$_2$ Nanoparticles. *J. Am. Chem. Soc.* **2012**, *134*, 7600–7603. [CrossRef]

73. Zhang, S.; Zheng, H.; Sun, Y.; Li, F.; Li, T.; Liu, X.; Zhou, Y.; Chen, W.; Ju, H. Oxygen vacancies enhanced photoelectrochemical aptasensing of 2, 3', 5, 5'-tetrachlorobiphenyl amplified with Ag$_3$VO$_4$ nanoparticle-TiO$_2$ nanotube array heterostructure. *Biosens. Bioelectron.* **2020**, *167*, 112477. [CrossRef] [PubMed]

74. Cui, Z.; Guo, S.; Yan, J.; Li, F.; He, W. BiOBr nanosheets with oxygen vacancies and lattice strain for enhanced photoelectrochemical sensing of doxycycline. *Appl. Surf. Sci.* **2020**, *512*, 145695. [CrossRef]

75. Wang, H.; Zhang, B.; Wang, C.; Xi, J.; Zhao, F.; Zeng, B. Tailoring the Surface Oxygen Vacancies in Nanoporous BiOCl$_{0.8}$I$_{0.2}$ Nanoflowers for Photocathodic Sensing. *ACS Appl. Nano Mater.* **2020**, *3*, 6423–6431. [CrossRef]

76. Yan, P.; Dong, J.; Mo, Z.; Xu, L.; Qian, J.; Xia, J.; Zhang, J.; Li, H. Enhanced photoelectrochemical sensing performance of graphitic carbon nitride by nitrogen vacancies engineering. *Biosens. Bioelectron.* **2020**, *148*, 111802. [CrossRef]

77. Wang, H.; Zhang, L.; Chen, Z.; Hu, J.; Li, S.; Wang, Z.; Liu, J.; Wang, X. Semiconductor heterojunction photocatalysts: Design, construction, and photocatalytic performances. *Chem. Soc. Rev.* **2014**, *43*, 5234–5244. [CrossRef]

78. Zhang, L.; Jiang, D.; Shan, X.; Du, X.; Wei, M.; Zhang, Y.; Chen, Z. Visible light-driven self-powered aptasensors for ultrasensitive Microcystin-LR detection based on the carrier density effect of N-doped graphene hydrogel/hematite Schottky junctions. *Analyst* **2021**, *146*, 6220–6227. [CrossRef]

79. Li, M.Y.; Zhang, G.X.; Feng, C.Q.; Wu, H.M.; Mei, H. Highly sensitive detection of chromium (VI) by photoelectrochemical sensor under visible light based on Bi SPR-promoted BiPO$_4$/BiOI heterojunction. *Sens. Actuator B-Chem.* **2020**, *305*, 127449. [CrossRef]

80. Zhao, M.; Yang, L.; Jiang, J.; Shi, N.; Huo, W.; Zhao, Z.; Yang, R.; Wang, J.; Zhao, Z.; Li, G.; et al. Highly Sensitive Detection of Ciprofloxacin by Photoelectrochemical Sensor Under Visible Light Based on BiPO$_4$/BiOI Heterojunction. *J. Electrochem. Soc.* **2019**, *166*, B1742. [CrossRef]

81. Xu, L.; Jiang, D.; Zhao, Y.; Yan, P.; Dong, J.; Qian, J.; Ao, H.; Li, J.; Yan, C.; Li, H. Integrated BiPO$_4$ nanocrystal/BiOBr heterojunction for sensitive photoelectrochemical sensing of 4-chlorophenol. *Dalton Trans.* **2018**, *47*, 13353–13359. [CrossRef] [PubMed]

82. Qian, J.; Yang, Z.; Wang, C.; Wang, K.; Liu, Q.; Jiang, D.; Yan, Y.; Wang, K. One-pot synthesis of BiPO$_4$ functionalized reduced graphene oxide with enhanced photoelectrochemical performance for selective and sensitive detection of chlorpyrifos. *J. Mater. Chem. A* **2015**, *3*, 13671–13678. [CrossRef]

83. Zhang, Z.X.; Zhai, L.Y.; Li, M.Q.; Wu, J.H.; Li, L. A novel RGO/BiVO$_4$ photoelectrochemical sensor for tetracycline hydrochloride detection. *Chem. Phys. Lett.* **2023**, *814*, 140291. [CrossRef]

84. Qi, X.; Tao, S. MWCNT modified Ni–Fe LDH/BiVO$_4$ heterojunction: Boosted visible-light-driven photoelectrochemical aptasensor for ofloxacin detection. *RSC Adv.* **2022**, *12*, 24269–24277. [CrossRef]

85. Cheng, Y.; Chen, C.; Hu, S.; Liu, X.; Zhang, L.; Huang, W.; Song, S.; Xia, L. A Facile Photoelectrochemical Sensor for High Sensitive Dopamine and Ascorbic Acid Detection Based on Bi surface Plasmon Resonance-Promoted BiVO$_4$ Microspheres. *J. Electrochem. Soc.* **2020**, *167*, 027536. [CrossRef]

86. Hao, N.; Chen, S.B.; Qian, J.; Zhang, Y.; Liu, Q.; Zhang, X.; Wang, K. A sensitive photoelectrochemical (PEC) platform fabricated with nitrogen doped graphene quantum dots decorated Bi$_2$WO$_6$ for detection of pentachlorophenol. *J. Electroanal. Chem.* **2017**, *801*, 410–415. [CrossRef]

87. Li, Y.; Yu, X.; Li, R.; Zhao, F.; Liu, G.; Wang, X. Selective and sensitive visible-light-prompt photoelectrochemical sensor of paracetamol based on Bi$_2$WO$_6$ modified with Bi and copper sulfide. *RSC Adv.* **2021**, *11*, 2884–2891. [CrossRef]

88. Tong, M.; Zhang, N.; Tan, Z.; Chi, L.; Zhang, K.; Chen, B.; Hu, F.; Guo, C. Oxygen vacancy-rich Bi$_2$WO$_6$ nanocrystals for fast and wide-range photoelectrochemical sensing of hydrogen peroxide. *Microchem. J.* **2023**, *190*, 108618. [CrossRef]

89. Ge, L.; Xu, Y.H.; Ding, L.J.; You, F.H.; Liu, Q.; Wang, K. Perovskite-type BiFeO$_3$/ultrathin graphite-like carbon nitride nanosheets p-n heterojunction: Boosted visible-light-driven photoelectrochemical activity for fabricating ampicillin aptasensor. *Biosens. Bioelectron.* **2019**, *124*, 33–39. [CrossRef]

90. Zhou, Q.; Lin, Y.; Zhang, K.; Li, M.; Tang, D. Reduced graphene oxide/BiFeO$_3$ nanohybrids-based signal-on photoelectrochemical sensing system for prostate-specific antigen detection coupling with magnetic microfluidic device. *Biosens. Bioelectron.* **2018**, *101*, 146–152. [CrossRef] [PubMed]

91. Pang, Y.; Li, Y.; Xu, G.; Hu, Y.; Kou, Z.; Feng, Q.; Lv, J.; Zhang, Y.; Wang, J.; Wu, Y. Z-scheme carbon-bridged Bi$_2$O$_3$/TiO$_2$ nanotube arrays to boost photoelectrochemical detection performance. *Appl. Catal. B* **2019**, *248*, 255–263. [CrossRef]

92. Li, G.; Zhang, D.; Yu, J.C.; Leung, M.K.H. An Efficient Bismuth Tungstate Visible-Light-Driven Photocatalyst for Breaking Down Nitric Oxide. *Environ. Sci. Technol.* **2010**, *44*, 4276–4281. [CrossRef] [PubMed]

93. Adhikari, S.; Kim, D.-H. Synthesis of Bi$_2$S$_3$/Bi$_2$WO$_6$ hierarchical microstructures for enhanced visible light driven photocatalytic degradation and photoelectrochemical sensing of ofloxacin. *Chem. Eng. J.* **2018**, *354*, 692–705. [CrossRef]

94. Wang, Y.; Zu, M.; Zhou, X.; Lin, H.; Peng, F.; Zhang, S. Designing efficient TiO$_2$-based photoelectrocatalysis systems for chemical engineering and sensing. *Chem. Eng. J.* **2020**, *381*, 122605. [CrossRef]

95. Shen, S.; Chen, J.; Wang, M.; Sheng, X.; Chen, X.; Feng, X.; Mao, S.S. Titanium dioxide nanostructures for photoelectrochemical applications. *Prog. Mater. Sci.* **2018**, *98*, 299–385. [CrossRef]

96. Kang, Q.; Yang, L.; Chen, Y.; Luo, S.; Wen, L.; Cai, Q.; Yao, S. Photoelectrochemical detection of pentachlorophenol with a Multiple Hybrid CdSe$_x$Te$_{1−x}$/TiO$_2$ Nanotube Structure-Based Label-Free Immunosensor. *Anal. Chem.* **2010**, *82*, 9749–9754. [CrossRef]

97. Gao, B.; Zhao, X.; Liang, Z.; Wu, Z.; Wang, W.; Han, D.; Niu, L. CdS/TiO$_2$ Nanocomposite-Based Photoelectrochemical Sensor for a Sensitive Determination of Nitrite in Principle of Etching Reaction. *Anal. Chem.* **2021**, *93*, 820–827. [CrossRef]

98. Jia, S.; Li, X.; Zhang, B.; Yang, J.; Zhang, S.; Li, S.; Zhang, Z. TiO$_2$/CuS heterostructure nanowire array photoanodes toward water oxidation: The role of CuS. *Appl. Surf. Sci.* **2019**, *463*, 829–837. [CrossRef]

99. Jena, A.; Chen, C.-J.; Chang, H.; Hu, S.-F.; Liu, R.-S. Comprehensive view on recent developments in hydrogen evolution using MoS$_2$ on a Si photocathode: From electronic to electrochemical aspects. *J. Mater. Chem. A* **2021**, *9*, 3767–3785. [CrossRef]

100. Wei, J.; Qileng, A.; Yan, Y.; Lei, H.; Zhang, S.; Liu, W.; Liu, Y. A novel visible-light driven photoelectrochemical immunosensor based on multi-amplification strategy for ultrasensitive detection of microcystin-LR. *Anal. Chim. Acta* **2017**, *994*, 82–91. [CrossRef]

101. Liu, Q.; Shi, T.; Cheng, Y.; Wen, Z.; Ding, C.; Li, Y.; Wang, K. Amplified photocurrent signal for fabricating photoelectrochemical sulfadimethoxine aptasensor based on carbon nitride photosensitization with visible/near-infrared light responsive zinc phthalocyanine. *J. Hazard. Mater.* **2021**, *406*, 124749. [CrossRef]

102. Wang, J.; Liu, Z. Recent advances in two-dimensional layered materials for photoelectrochemical sensing. *Trac-Trends Anal. Chem.* **2020**, *133*, 116089. [CrossRef]

103. Chen, Y.; Wang, Y.; Yan, P.; Ouyang, Q.; Dong, J.; Qian, J.; Chen, J.; Xu, L.; Li, H. Co$_3$O$_4$ nanoparticles/graphitic carbon nitride heterojunction for photoelectrochemical aptasensor of oxytetracycline. *Anal. Chim. Acta* **2020**, *1125*, 299–307. [CrossRef]

104. Liu, J.; Yan, K.; Zhang, J. A biophotoelectrocatalytic system for pollutant removal based on carbon fiber cloth supported TiO$_2$ photoanode with oxygen vacancy defects and CuO/g-C$_3$N$_4$ photocathode. *Carbon* **2022**, *200*, 410–421. [CrossRef]

105. Liu, M.; Yu, J.; Ding, X.; Zhao, G. Photoelectrochemical Aptasensor for the Sensitive Detection of Microcystin-LR Based on Graphene Functionalized Vertically-aligned TiO$_2$ Nanotubes. *Electroanalysis* **2016**, *28*, 161–168. [CrossRef]

106. do Prado, T.M.; Cincotto, F.H.; Fatibello-Filho, O.; Cruz de Moraes, F. Bismuth Vanadate/Reduced Graphene Oxide Nanocomposite Electrode for Photoelectrochemical Determination of Diclofenac in Urine. *Electroanalysis* **2018**, *30*, 2704–2711. [CrossRef]

107. Lu, H.; Wang, G.; Dai, R.; Ding, X.; Liu, M.; Sun, H.; Sun, C.; Zhao, G. Visible-light-driven photoelectrochemical aptasensor based on reduced graphene oxide/Ti–Fe–O nanotube arrays for highly sensitive and selective determination of microcystin-LR. *Electrochim. Acta* **2019**, *324*, 134820. [CrossRef]

108. Zhang, Z.; Zhang, M.; Xu, Y.; Wen, Z.; Ding, C.; Guo, Y.; Hao, N.; Wang, K. $Bi^{3+}$ engineered black anatase titania coupled with graphene for effective tobramycin photoelectrochemical detection. *Sens. Actuator B-Chem.* **2020**, *321*, 128464. [CrossRef]

109. Zhou, Y.; Yin, H.; Ai, S. Applications of two-dimensional layered nanomaterials in photoelectrochemical sensors: A comprehensive review. *Coordin. Chem. Rev.* **2021**, *447*, 214156. [CrossRef]

110. Seo, D.-B.; Trung, T.N.; Bae, S.-S.; Kim, E.-T. Improved Photoelectrochemical Performance of $MoS_2$ through Morphology-Controlled Chemical Vapor Deposition Growth on Graphene. *Nanomaterials* **2021**, *11*, 1585. [CrossRef]

111. Salem, M.; Akir, S.; Massoudi, I.; Litaiem, Y.; Gaidi, M.; Khirouni, K. Photoelectrochemical and optical properties tuning of graphene-ZnO nanocomposites. *J. Alloy. Compd.* **2018**, *767*, 982–987. [CrossRef]

112. Wang, B.; Huang, Z.; Tang, P.; Luo, S.; Liu, Y.; Li, J.; Qi, X. One-pot synthesized $Bi_2Te_3$/graphene for a self-powered photoelectrochemical-type photodetector. *Nanotechnology* **2020**, *31*, 115201. [CrossRef] [PubMed]

113. Yan, K.; Liu, Y.; Yang, Y.; Zhang, J. A Cathodic "Signal-off" Photoelectrochemical Aptasensor for Ultrasensitive and Selective Detection of Oxytetracycline. *Anal. Chem.* **2015**, *87*, 12215–12220. [CrossRef] [PubMed]

114. Hao, N.; Zhang, X.; Zhou, Z.; Qian, J.; Liu, Q.; Chen, S.; Zhang, Y.; Wang, K. Three-dimensional nitrogen-doped graphene porous hydrogel fabricated biosensing platform with enhanced photoelectrochemical performance. *Sens. Actuator B-Chem.* **2017**, *250*, 476–483. [CrossRef]

115. Jiang, D.; Du, X.; Liu, Q.; Hao, N.; Wang, K. $MoS_2$/nitrogen doped graphene hydrogels p-n heterojunction: Efficient charge transfer property for highly sensitive and selective photoelectrochemical analysis of chloramphenicol. *Biosens. Bioelectron.* **2019**, *126*, 463–469. [CrossRef] [PubMed]

116. Peng, J.; Huang, Q.; Zhuge, W.; Liu, Y.; Zhang, C.; Yang, W.; Xiang, G. Blue-light photoelectrochemical sensor based on nickel tetra-amined phthalocyanine-graphene oxide covalent compound for ultrasensitive detection of erythromycin. *Biosens. Bioelectron.* **2018**, *106*, 212–218. [CrossRef]

117. Tayebi, M.; Kolaei, M.; Tayyebi, A.; Masoumi, Z.; Belbasi, Z.; Lee, B.-K. Reduced graphene oxide (RGO) on $TiO_2$ for an improved photoelectrochemical (PEC) and photocatalytic activity. *Sol. Energy* **2019**, *190*, 185–194. [CrossRef]

118. Tian, J.; Zhao, H.; Quan, X.; Zhang, Y.; Yu, H.; Chen, S. Fabrication of graphene quantum dots/silicon nanowires nanohybrids for photoelectrochemical detection of microcystin-LR. *Sens. Actuator B-Chem.* **2014**, *196*, 532–538. [CrossRef]

119. Liu, M.; Ding, X.; Yang, Q.; Wang, Y.; Zhao, G.; Yang, N. A pM leveled photoelectrochemical sensor for microcystin-LR based on surface molecularly imprinted $TiO_2$@CNTs nanostructure. *J. Hazard. Mater.* **2017**, *331*, 309–320. [CrossRef]

120. Li, Y.; Bu, Y.; Jiang, F.; Dai, X.; Ao, J.-P. Fabrication of ultra-sensitive photoelectrochemical aptamer biosensor: Based on semiconductor/DNA interfacial multifunctional reconciliation via 2D-$C_3N_4$. *Biosens. Bioelectron.* **2020**, *150*, 111903. [CrossRef]

121. Hou, W.; Cronin, S.B. A Review of Surface Plasmon Resonance-Enhanced Photocatalysis. *Adv. Funct. Mater.* **2013**, *23*, 1612–1619. [CrossRef]

122. Zhou, X.; Liu, G.; Yu, J.; Fan, W. Surface plasmon resonance-mediated photocatalysis by noble metal-based composites under visible light. *J. Mater. Chem.* **2012**, *22*, 21337–21354. [CrossRef]

123. Tan, J.; Peng, B.; Tang, L.; Feng, C.; Wang, J.; Yu, J.; Ouyang, X.; Zhu, X. Enhanced photoelectric conversion efficiency: A novel h-BN based self-powered photoelectrochemical aptasensor for ultrasensitive detection of diazinon. *Biosens. Bioelectron.* **2019**, *142*, 111546. [CrossRef]

124. Pei, F.; Feng, S.; Zhang, Y.; Wu, Y.; Chen, C.; Sun, Y.; Xie, Z.; Hao, Q.; Cao, Y.; Tong, Z.; et al. A photoelectrochemical immunosensor based on Z-scheme CdS composite heterojunction for aflatoxin $B_1$. *Biosens. Bioelectron.* **2022**, *214*, 114500. [CrossRef] [PubMed]

125. Xu, L.; Ling, S.; Li, H.; Yan, P.; Xia, J.; Qiu, J.; Wang, K.; Li, H.; Yuan, S. Photoelectrochemical monitoring of 4-chlorophenol by plasmonic Au/graphitic carbon nitride composites. *Sens. Actuator B-Chem.* **2017**, *240*, 308–314. [CrossRef]

126. Geng, H.; Chen, X.; Sun, L.; Qiao, Y.; Song, J.; Shi, S.; Cai, Q. ZnCuInSe/Au/$TiO_2$ sandwich nanowires-based photoelectrochemical biosensor for ultrasensitive detection of kanamycin. *Anal. Chim. Acta* **2021**, *1146*, 166–173. [CrossRef]

127. Zhang, Z.; Ding, X.; Lu, G.; Du, B.; Liu, M. A highly sensitive and selective photoelectrochemical aptasensor for atrazine based on Au NPs/3DOM $TiO_2$ photonic crystal electrode. *J. Hazard. Mater.* **2023**, *451*, 131132. [CrossRef]

128. Wang, C.; Zhao, Y.; Xu, L.; Yan, P.; Qian, J.; Zhao, L.; Zhang, J.; Li, H. Specific electron-transfer and surface plasmon resonance integrated boosting visible-light photoelectrochemical sensor for 4-chlorophenol. *J. Electroanal. Chem.* **2019**, *833*, 251–257. [CrossRef]

129. Yang, S.; Deng, K.; Zhang, J.; Bai, C.; Peng, J.; Fang, Z.; Xu, W. Synergy effect of Ag plasmonic resonance and heterostructure construction enhanced visible-light photoelectrochemical sensing for quercetin. *Electrochim. Acta* **2021**, *371*, 137772. [CrossRef]

130. Zhu, J.-H.; Feng, Y.-G.; Wang, A.-J.; Mei, L.-P.; Luo, X.; Feng, J.-J. A signal-on photoelectrochemical aptasensor for chloramphenicol assay based on 3D self-supporting AgI/Ag/BiOI Z-scheme heterojunction arrays. *Biosens. Bioelectron.* **2021**, *181*, 113158. [CrossRef]

131. Zhang, J.; Zhang, X.; Gao, Y.; Yan, J.; Song, W. Integrating CuO/g-$C_3N_4$ p-n heterojunctioned photocathode with $MoS_2$ QDs@Cu NWs multifunctional signal amplifier for ultrasensitive detection of AβO. *Biosens. Bioelectron.* **2021**, *176*, 112945. [CrossRef] [PubMed]

132. Peng, J.; Zhuge, W.; Liu, Y.; Zhang, C.; Yang, W.; Huang, Y. Photoelectrochemical Dopamine Sensor Based on Cu-Doped $Bi_2WO_6$ Micro-Flowers Sensitized Cobalt Tetraaminophthalocyanine Functionalized Graphene Oxide. *J. Electrochem. Soc.* **2019**, *166*, B1612–B1619. [CrossRef]

133. Wen, Z.; Zhu, W.; You, F.; Yuan, R.; Ding, L.; Hao, N.; Wei, J.; Wang, K. Ultrasensitive photoelectrochemical aptasensor for carbendazim detection based on in-situ constructing Schottky junction via photoreducing Pd nanoparticles onto CdS microsphere. *Biosens. Bioelectron.* **2022**, *203*, 114036. [CrossRef] [PubMed]

134. Zhang, C.; Zhou, L.; Peng, J. Blue-light photoelectrochemical aptasensor for kanamycin based on synergistic strategy by Schottky junction and sensitization. *Sens. Actuator B-Chem.* **2021**, *340*, 129898. [CrossRef]

135. Zhang, Y.; Zhu, Y.; Zeng, T.; Qiao, L.; Zhang, M.; Song, K.; Yin, N.; Tao, Y.; Zhao, Y.; Zhang, C.; et al. Self-powered photoelectrochemical aptasensor based on hollow tubular g-$C_3N_4$/Bi/$BiVO_4$ for tobramycin detection. *Anal. Chim. Acta* **2023**, *1250*, 340951. [CrossRef]

136. Xu, Y.; Jiang, D.; Zhang, M.; Zhang, Z.; Qian, J.; Hao, N.; Ding, C.; Wang, K. High-performance photoelectrochemical aptasensor for enrofloxacin based on Bi-doped ultrathin polymeric carbon nitride nanocomposites with SPR effect and carbon vacancies. *Sens. Actuator B-Chem.* **2020**, *316*, 128142. [CrossRef]

137. Tian, Y.; Cui, Q.; Xu, L.; Jiao, A.; Ma, H.; Wang, C.; Zhang, M.; Wang, X.; Li, S.; Chen, M. Alloyed AuPt nanoframes loaded on h-BN nanosheets as an ingenious ultrasensitive near-infrared photoelectrochemical biosensor for accurate monitoring glucose in human tears. *Biosens. Bioelectron.* **2021**, *192*, 113490. [CrossRef]

138. Tang, L.; Ouyang, X.; Peng, B.; Zeng, G.; Zhu, Y.; Yu, J.; Feng, C.; Fang, S.; Zhu, X.; Tan, J. Highly sensitive detection of microcystin-LR under visible light using a self-powered photoelectrochemical aptasensor based on a CoO/Au/g-$C_3N_4$ Z-scheme heterojunction. *Nanoscale* **2019**, *11*, 12198–12209. [CrossRef] [PubMed]

139. Okoth, O.K.; Yan, K.; Feng, J.; Zhang, J. Label-free photoelectrochemical aptasensing of diclofenac based on gold nanoparticles and graphene-doped CdS. *Sens. Actuator B-Chem.* **2018**, *256*, 334–341. [CrossRef]

140. Altın, İ.; Sökmen, M.; Bıyıklıoğlu, Z. Sol gel synthesis of cobalt doped $TiO_2$ and its dye sensitization for efficient pollutant removal. *Mater. Sci. Semicond. Process.* **2016**, *45*, 36–44. [CrossRef]

141. Lima, F.M.D.; Freires, A.D.; Pereira, N.D.; Silva, G.G.; da Rocha, C.Q.; Damos, F.S.; Luz, R.D.S. Photoelectrochemical sensing of tannic acid based on the use of $TiO_2$ sensitized with 5-methylphenazinium methosulfate and carboxy-functionalized CdTe quantum dots. *Microchim. Acta* **2018**, *185*, 521. [CrossRef] [PubMed]

142. Sousa, C.S.; Lima, K.; Botelho, C.N.; Pereira, N.M.; Fernandes, R.N.; Silva, G.G.; Damos, F.S.; Luz, R.C.S. Photoelectrochemical sensor for determination of naringin at low oxidation potential using a modified FTO electrode with cadmium sulfide and titanium dioxide sensitized with chloroprotoporphyrin IX iron(III). *J. Solid State Electrochem.* **2020**, *24*, 1715–1726. [CrossRef]

143. Wei, J.; Xie, X.; Chang, W.; Yang, Z.; Liu, Y. Ultrasensitive photoelectrochemical detection of microcystin-LR based on hybridization chain reaction assisted exciton-plasmon interaction and enzymatic biocatalytic precipitation. *Sens. Actuator B-Chem.* **2018**, *276*, 180–188. [CrossRef]

144. Botelho, C.N.; Pereira, N.D.M.; Silva, G.G.; Silva de Menezes, A.; Brito Bezerra, C.W.; Damos, F.S.; Luz, R.D.C.S. Photoelectrochemical-assisted determination of caffeic acid exploiting a composite based on carbon nanotubes, cadmium telluride quantum dots, and titanium dioxide. *Anal. Method* **2019**, *11*, 4775–4784. [CrossRef]

145. Yan, T.; Ding, H.; Feng, R.; Yuan, R.; Zhao, Y.; Sun, M.; Yan, L.; Wei, Q. Self-powered Aptasensors Made with the $In_2O_3$–$In_2S_3$–$Ti_3C_2$ Composite for Dual-mode Detection of Microcystin-LR. *ACS Appl. Mater. Interfaces* **2022**, *14*, 25308–25316. [CrossRef] [PubMed]